

NATIONAL TRANSPORTATION SAFETY BOARD

Office of Research and Engineering
Materials Laboratory Division
Washington, D.C. 20594



January 3, 2022

MATERIALS LABORATORY FACTUAL REPORT

Report No. 21-091

A. ACCIDENT INFORMATION

Place : Daytona Beach, Florida
Date : April 4, 2018
Vehicle : Piper PA-28R-201, N106ER
NTSB No. : ERA18FA120
Investigator : Aaron McCarter, AS-ERA / Clinton R. Crookshanks, AS-40

B. COMPONENTS EXAMINED

3 exemplar left wing main spar lower spar cap pieces with confirmed crack indications removed from the following airplanes:

Spar A from a Piper PA-28RT-201T, S/N 28R-7931247

Spar B from a Piper PA-28R-201, S/N 2844098

Spar C from a Piper PA-32-300, S/N 32-40456

C. DETAILS OF THE EXAMINATION

The inboard ends of 3 main spar lower spar caps with attached doubler pieces were received for examination as shown in figure 1. For reference in this report, the spars were labeled A through C as noted above. The spars were part of the left wing structure on three airplanes having model numbers and serial numbers affected by Federal Aviation Administration Airworthiness Directive (AD) 2020-26-16, which requires an eddy current bolt hole inspection of main wing spar attachment bolt holes of certain airplanes. Each of the three spars had a crack indication that was detected through eddy current inspection followed by visual inspections and/or fluorescent penetrant inspections.

According to engineering drawings for the accident airplane, the main spar is an I-shaped extrusion of aluminum alloy 2024-T3511. As installed on the airplane, each wing spar is attached to the center wing box with 18 attachment bolts; 8 through the upper spar cap and 10 through the lower spar cap. In each spar cap, half of the bolts are located forward of the spar web, and the remaining bolts are located aft of the web. Doublers are riveted to the forward and aft sides of the spar at the attachment location and outboard beyond the bend in the spar that forms the wing dihedral. Flanges for the doublers extend over the upper and lower spar caps at the forward side of the spar and over the lower spar cap at the aft side of the spar.

For reference in this report, wing spar attachment bolt holes are labeled with three alphanumeric characters to identify their locations. The first letter in the identification is

an L to indicate the left wing. The second letter in the identification indicates the row of bolt holes consistent with the labeling convention used by Piper Aircraft Inc. For the lower spar cap, row C is located forward of the spar web and row D was located aft of the web. (Rows A and B are located in the upper spar cap.) Finally, the bolt holes in each row are identified with a number in sequence starting from the outboard bolt hole, also consistent with the labeling convention used by the aircraft manufacturer. As per the manufacturer convention, a dash is inserted between the row letter and the hole number.

The crack indications in each spar were located in the number 1 (outboard) holes. In spar A, the crack indication was located in the aft bolt hole (hole LD-1). A crack indication was located in the forward bolt hole (hole LC-1) in spars B and C.

Descriptions of findings for each spar are described in subsequent sections of this report. The numbers for the remaining figures are preceded by the spar letter to help distinguish the spar with which the figure is associated.

1. Spar A

An overall view of the lower surface of the spar A lower spar cap is shown in figure A1, and closer views of the outboard attachment holes are shown in figures A2 to A4. Deposits of reddish orange oxides, likely from the attachment bolt, were present on the interior of hole LC-1, particularly on the outboard half. A relatively large vertical scratch was also observed on the inboard forward quadrant of hole LC-1 as shown in figure A3.

A pit was observed on the outboard side of hole LC-1 as shown in figure A4. The spar piece was placed in a scanning electron microscope (SEM), and SEM images of the hole LC-1 surface at the pit are shown in figures A5. The pit had dimpled features with some mud cracking on the surface and oxide-filled areas, features consistent with a corrosion pit. The area around the pit was mostly covered by thicker iron oxides.

A crack was observed at the outboard aft quadrant of hole LD-1 as shown in figure A6. The crack intersected the lower surface to the extent indicated with a bracket in figure A6 and was observed intersecting part of the hole LD-1 bore. An SEM image of the area where the crack intersected hole LD-1 is shown in figure A7. Corrosion pits were observed on the hole LD-1 bore near the crack as indicated in figure A7.

Next, a line of cyanoacrylate gel adhesive was applied to the trailing edge at the joint between the doubler and the spar piece and was allowed to dry. Then the spar was sectioned longitudinally through the hole LD-1 through 5 axes to facilitate a direct view of the hole bores. A view of the LD-1 bore after sectioning is shown in figure A8. The crack was visible at the lower end of the hole bore as indicated in figure A8. No crack was detected in the upper portion of the hole bore through the spar cap or in the doubler on the upper side of the spar cap.

After the hole bores had been examined, the doubler was removed from the spar along the aft side of the attachment holes by soaking the sectioned piece in acetone to

dissolve the adhesive that had been applied to the trailing edge. Then to expose the crack fracture surfaces, a V-shaped section was cut from the trailing edge of the spar toward the visible crack tip on the lower surface, and the crack was opened by lab fracture. The inboard side of the crack was then cleaned by applying acetate tape to remove loose oxides and deposits followed by ultrasonic cleaning while submerged in acetone. An optical image of the crack surface after the initial cleaning is shown in figure A9. The image was acquired with a Keyence VHX-7000 microscope using a depth-up focus function.¹ Radial features and curving crack arrest lines consistent with fatigue emanated from an origin area at the lower edge of the fracture surface aft of hole LD-1 as indicated in figure A9. A dashed line in figure A9 indicates the fatigue crack boundary, which extended 0.140 inch aft of the hole at the lower surface and 0.076 inch upward from the lower surface at the hole LD-1 bore.

The fracture surface was then examined using the SEM, and an SEM image of the fatigue origin area is shown in figure A10. Unlabeled arrows in figure A10 indicate general directions of crack propagation away from the origin area that was mostly obscured by oxides and deposits. The oxides at the origin area were analyzed using energy dispersive x-ray spectroscopy (EDS), and a typical spectrum is shown in figure A11. The EDS spectrum of the oxides and deposits at the origin area included a small peak of chlorine.

An SEM image of fracture features at the fatigue boundary is shown in figure A12. Unlabeled arrows in figure A12 indicate multiple relatively prominent crack arrest lines that were observed at relatively low magnification. A distinct change in fracture features was observed between the last prominent arrest line and the boundary, which could indicate a change in airplane usage or storage environment.

Fracture features across most of the fatigue region were substantially damaged with faceted impressions and rubbed features. An SEM image of the fracture surface in the damaged area is shown in figure A13. Multiple faceted nonconductive particles were found embedded in the damaged surface, and EDS analyses of the particles had spectra such as those shown in figure A14. High peaks of aluminum and oxygen consistent with aluminum oxide (corundum) were observed on some faceted particles, and others had high peaks of silicon and oxygen consistent with silica (quartz).

The inboard side of the lab fracture was cleaned using a heated aqueous solution of chromic acid and phosphoric acid for removing oxides on aluminum. An optical image of the fatigue region after oxide removal is shown in figure A15, and a montage of SEM images of the same area is shown in figure A16. A fatigue origin was observed on the lower surface approximately 0.012 inch away from the hole bore as indicated in figures A17 and A18. The origin area was damaged by corrosion pitting. However the surface showed hints of fine radial features emanating from a semi-circular pitted area that measured up to 0.0006 inch deep.

¹ The depth-up focus function constructs an image from a series of images with different areas in focus to digitally enhance the depth of field.

Striations and crack arrest lines consistent with fatigue crack growth under spectrum loading conditions were observed on the fracture surface as shown in figures A19 to A22. The images were generally taken along a path indicated with a dashed line in figure A16. Many of the finer fracture features were obscured or destroyed by post-fracture damage from hard particles or oxidation, particularly near the origin area.

Spar A was removed from an airplane that was manufactured in 1979. Registration records online indicate the airplane changed ownership in January 2003 from an owner in Oklahoma, United States to an owner in the United Kingdom. Pictures available online indicate the airplane was repainted sometime between August 25, 2017 and June 24, 2018. Another picture online showed the airplane without a propeller installed while parked outside in the United Kingdom at Perth airport on October 11, 2020. An ad was found online on December 11, 2021, indicating the airplane had been recently sold. The ad stated the airplane was up to date on its annual inspections until April 2022 and had 5,959 hours on the airframe.

2. Spar B

Views of the lower surface of the spar B piece are shown in figure B1. A crack was observed at the forward side hole LC-1 and was visible on the lower surface forward to the spar leading edge as shown in figure B2.

Next, a line of cyanoacrylate gel adhesive was applied to the leading edge between the doubler and the spar piece and was allowed to dry. Then the spar was sectioned longitudinally through the hole LC-1 through 5 axes to facilitate a direct view of the hole bores. A view of the crack in the forward side of the hole LC-1 bore after sectioning is shown in figure B3. The crack was visible intersecting the hole surface along the entire length of the hole in the spar. No crack was detected in the doubler on the upper side of the spar cap.

Next, the sectioned piece with the leading edge was soaked in acetone to remove the doubler by dissolving the adhesive. The crack faces then separated from each other once the doubler was removed. The inboard side of the crack was then cleaned by applying acetate tape to remove loose oxides and deposits followed by ultrasonic cleaning while submerged in acetone. A view of the fracture surface after initial cleaning is shown in figure B4. Fracture features consistent with fatigue were observed across most of the fracture surface to the dashed line in Figure B4. A relatively prominent crack arrest line was observed near the middle of the fracture as indicated with unlabeled arrows in Figure B4. The crack lengths associated with the relatively prominent arrest line were 0.285 inch along the lower surface and 0.210 inch upward at the hole bore as indicated in figure B4.

The inboard fracture was examined using an SEM. Crack arrest lines and striations consistent with fatigue crack growth under spectrum loading conditions were observed. However, the area near the origin was obscured by oxidation and paint deposits. After an initial examination was complete, the inboard side of the fracture was

cleaned using a heated aqueous solution of chromic acid and phosphoric acid for removing oxides on aluminum.

A view of the fracture surface after oxide removal is shown in figure B5. Fatigue fracture features emanated from an origin area near the lower forward corner of hole LC-1. The fracture surface with oxides removed was then further examined using an SEM. A montage of SEM images to depict the entire fatigue region and a view of the origin area at higher magnification are shown in figure B6. Fine fracture features near the origin were mostly obliterated by oxidation damage on the fracture surface. However, radial features on the fracture surface and fatigue features in isolated intact fracture surface areas (dark gray areas in figure B6) near the origin emanated from an origin area at the hole LC-1 bore near the lower surface. The origin area appeared to be located at the lower end of a corrosion pit in the hole bore measuring up to 0.00035 inch deep.

Striations and crack arrest lines consistent with spectrum loading were observed on the fracture surface as shown in figures B7 through B12. The SEM images in figures B7 through B12 show snapshots of the fracture surface along a path indicated with a dashed line in figure B6 extending forward and upward from the origin. As noted in the figure captions, SEM images close to the origin were taken after oxides had been removed, and the remaining images were taken before the oxide removal. A relatively thick and continuous oxide had been observed on much of the area near the origin up to the crack arrest line associated with the oxide boundary indicated in figure B9. The relatively prominent crack arrest line indicated with arrows in figure B4 is shown in figure B11.

The lower forward corner of hole LC-1 was deformed slightly out of round and had vertical scratches as indicated in figures B13 and B14. Additionally, corrosion pits were observed on the hole LC-1 bore near the lower end as shown in figures B14 through B16. Secondary cracks were observed at the forward lower corner (see figure B15) and in corrosion pits in the hole LC-1 bore (see figure B16).

Oxides and corrosion pits on spar piece with the mating (outboard) side of the crack were examined using an SEM. The piece had been cleaned with acetone using an ultrasonic cleaner but had not been exposed to the oxide-removing solution. Corrosion pits and oxides were observed on the hole bore adjacent to the crack as shown in figure B17. One of the oxidized areas was randomly selected for analysis using EDS, and the resulting spectrum showed a peak of chlorine as indicated in figure B17.

Spar B was removed from an airplane that was manufactured in 2003. After a brief ownership by a corporation from Salt Lake City, Utah, the airplane was owned by a limited liability company (LLC) based in Scottsdale, Arizona from 2003 to 2008. The airplane was then owned by Embry-Riddle Aeronautical University (ERAU) for the next 7 years. The airplane was then owned by a leasing company from Daytona Beach for 3.5 years. The airplane was then owned for 2 years by another LLC from Decatur, Alabama before being sold to the current owner, also an LLC, in August 2020. Accumulated time on the airframe was 9,378 hours at the time of the crack find. Based on usage patterns for the

2018 accident ERAU airplane and assuming a similar usage for the airplane with spar B, the estimated time and flight cycles accumulated when owned by ERAU was estimated to be ~4,750 hours and ~4,200 flights.

3. Spar C

Views of the lower surface of the submitted spar C piece are shown in figure C1. A crack was observed at the forward side of hole LC-1 intersecting the lower surface and the entire length of the hole LC-1 bore on the forward side of the hole as shown in figures C1 and C2. No crack was detected in the doubler.

Multiple indications of plastic deformation were observed near the outboard holes on the spar C piece. The lower surface of the spar forward of hole LC-1 had a textured appearance consistent with plastic deformation associated with varying surface grain orientations. Additionally, linear surface texture features emanated from the crack at 45-degree angles consistent with deformation associated with plastic slip (slip bands). A slight dip in the leading edge was noted forward of hole LC-1 as indicated in figure C3, and longitudinal extrusion lines were curved at that location as indicated in figure C1. On the aft side of the spar shown in figure C4, the doubler had a slight S-shaped bend near hole D1 consistent with a compression buckle.

Next, a line of cyanoacrylate gel adhesive was applied to the leading edge between the doubler and the spar piece and was allowed to dry. Then the spar was sectioned longitudinally through the hole LC-1 through 5 axes to facilitate a direct view of the hole bores. After an initial look at the hole bores, the doubler was removed from the forward piece by soaking in acetone to dissolve the adhesive. A view of the crack in the forward side of the hole LC-1 bore is shown in figure C5 after sectioning and removing the doubler. The crack was visible intersecting the hole surface along the entire length of the hole in the spar as shown in figure C5 and extended forward from the hole on the lower and upper surfaces as shown in figures C6 and C7. At the lower end of hole LC-1, a series of parallel shallow cracks consistent with stress cracks were observed on the hole bore adjacent to the crack as indicated in figure C5. At the upper end of hole LC-1, the crack deviated inboard relative to the hole centerline. Deformed longitudinal extrusion lines consistent with plastic deformation were noted on both the lower and upper surfaces at the forward side of hole LC-1 as indicated in figures C6 and C7.

The forward side of the hole LC-1 bore and adjacent lower surface forward of the hole were examined using an SEM, and an oblique view of the lower forward corner of the hole is shown in figure C8. Nonconductive material (appearing white in figure C8) was observed in the crack at the lower forward corner of hole LC-1. The EDS spectrum of the nonconductive material in the crack opening included a small chlorine peak as shown in figure C9.

A V-shaped cut was made from the leading edge toward the ends of the crack visible on the upper and lower surfaces of the spar cap. The crack was then opened by lab fracture to expose the crack fracture surfaces. The inboard side of the crack was then cleaned by applying acetate tape to remove loose oxides and deposits followed by

ultrasonic cleaning while submerged in acetone. A 3-dimensional representation of the fracture surface as obtained using the depth-up feature on the Keyence VHX-7000 optical microscope is shown in figure C10. The fracture surface had relatively rough features that intersected surfaces at slant angles, features consistent with overstress fracture. Dark oxides and reflective areas were consistent with post-fracture rubbing and sliding contact between the faces.

The inboard side of the fracture was cleaned using a heated aqueous solution of chromic acid and phosphoric acid for removing oxides on aluminum, and the resulting fracture surface as obtained using the depth-up feature on the Keyence microscope is shown in figure C11. The overall fracture had a matte gray appearance consistent with ductile overstress fracture. A dashed line in figure C11 indicates the extent of the crack before lab fracture.

The inboard side of the crack fracture surface was examined using the SEM, and images showing typical fracture features are shown in figures C12 through C15. SEM images of the inboard side of the crack fracture surface showed dimples and sliding contact features consistent with ductile overstress fracture. No evidence of fatigue or any other progressive fracture mechanism was observed.

Spar C was removed from an airplane that was manufactured in 1968. According to registration records, the airplane was owned by individuals and companies located in Plant City, Florida since 1990. Based on information posted online and reviewed on November 11, 2021, the airframe had a total 5,240 hours, and the airworthiness directive for inspecting the wing spar was complied with in May 2021. The posting further stated the engine had 1,206 hours TIS since overhaul in 2005.

Matthew R. Fox, Ph.D.
Senior Materials Engineer

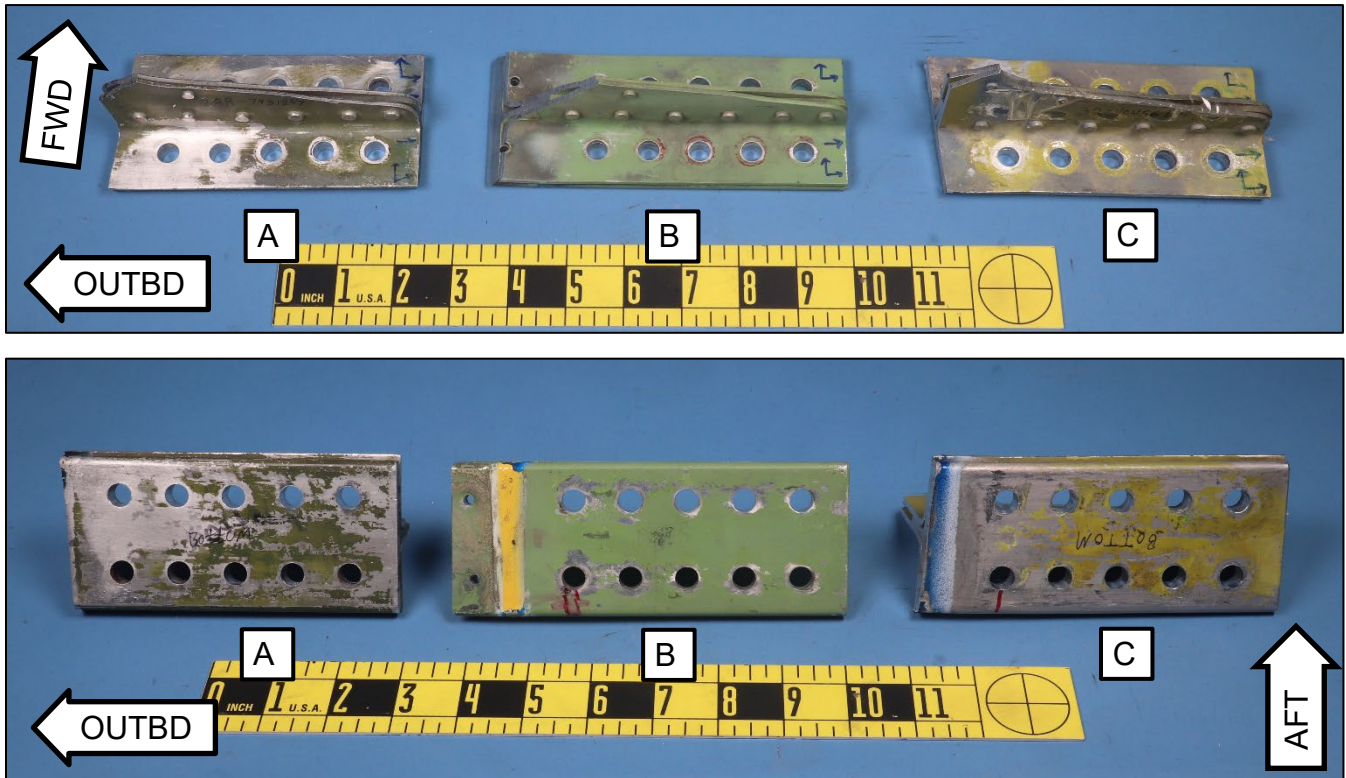


Figure 1. Overall views of the submitted main spar lower spar cap pieces.



Figure A1. Spar A lower surface.

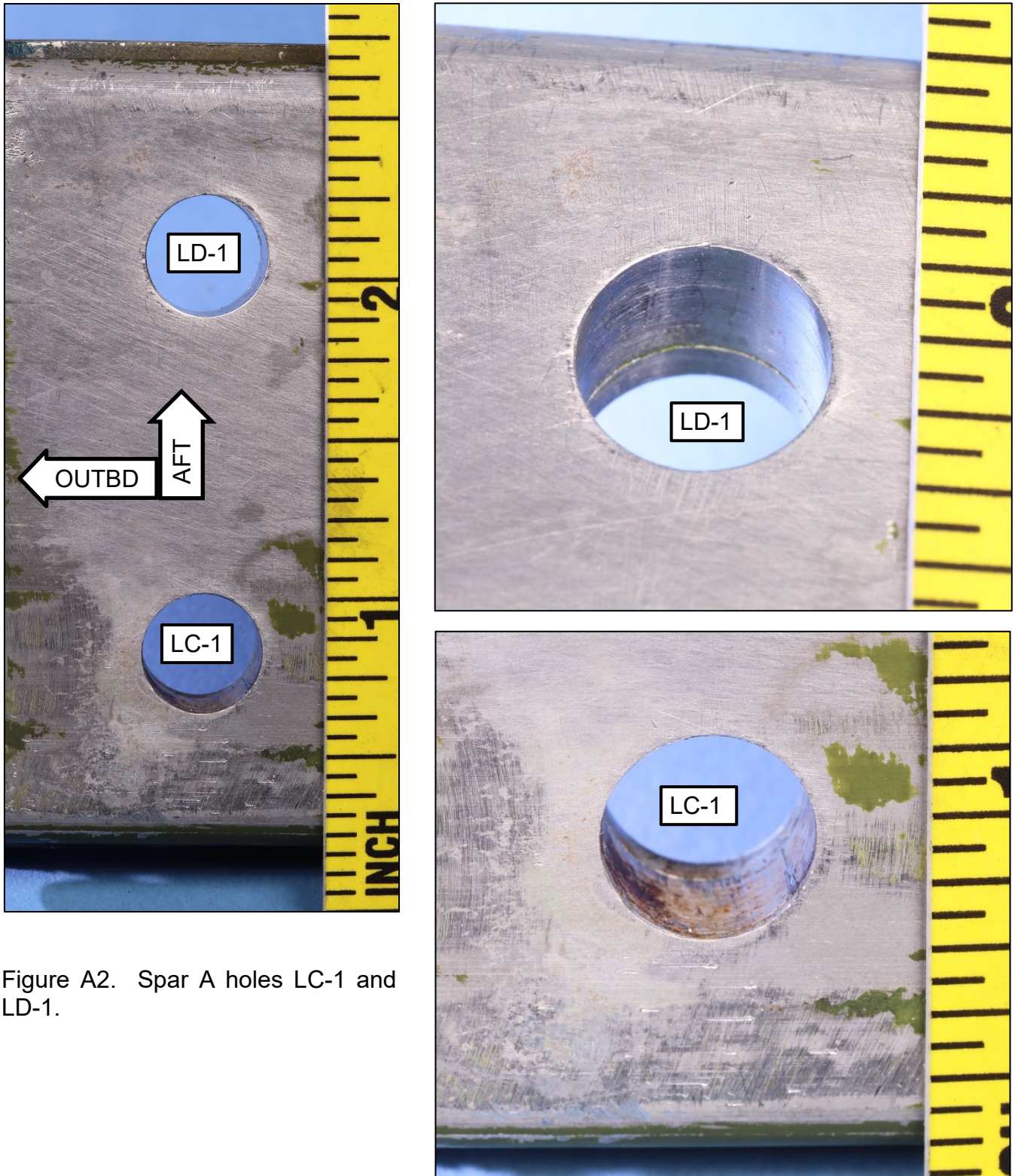


Figure A2. Spar A holes LC-1 and LD-1.

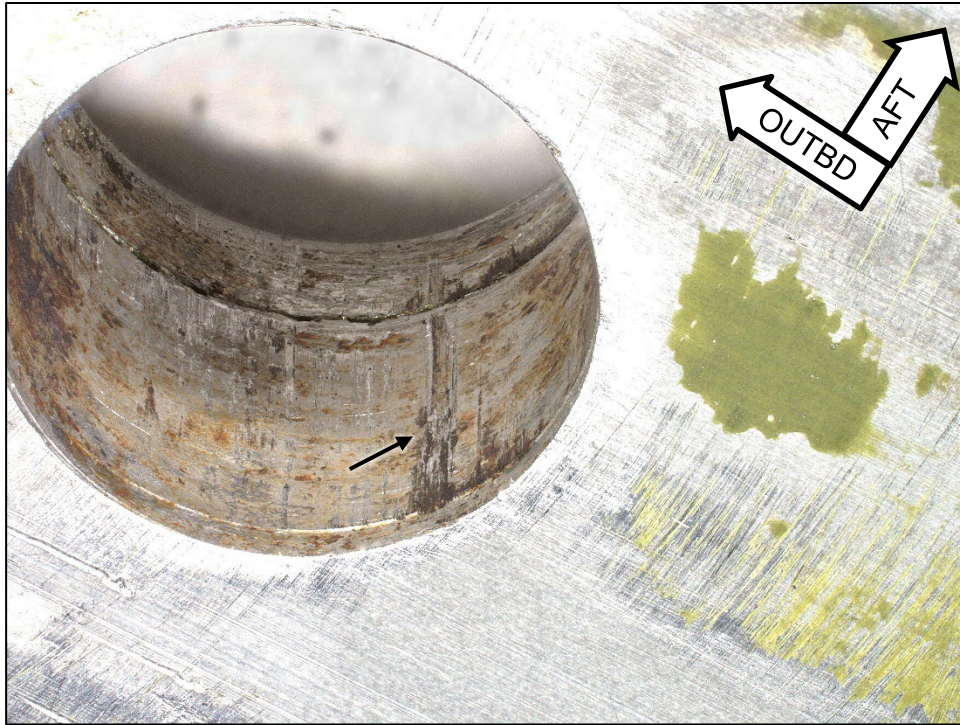


Figure A3. Scratch on the inboard forward quadrant of hole LC-1.

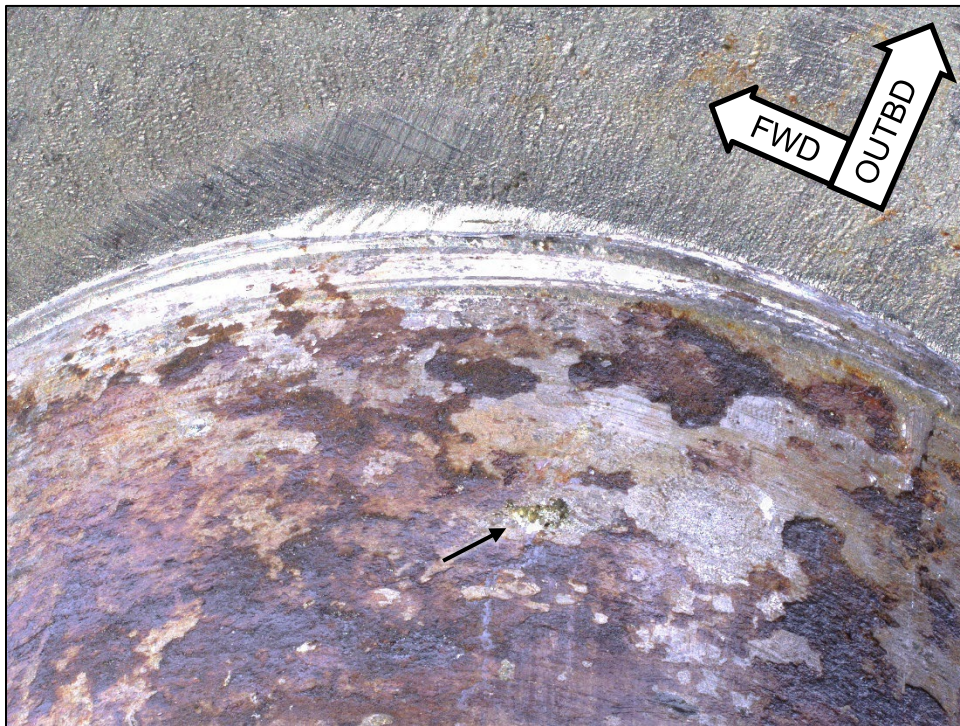


Figure A4. Pit on the outboard side of hole LC-1.

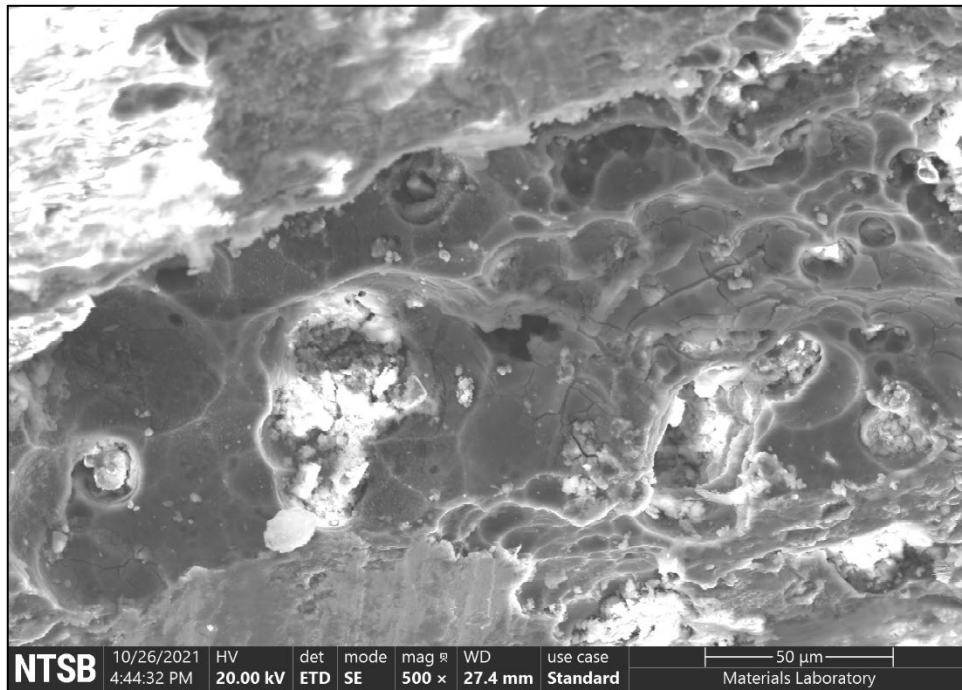
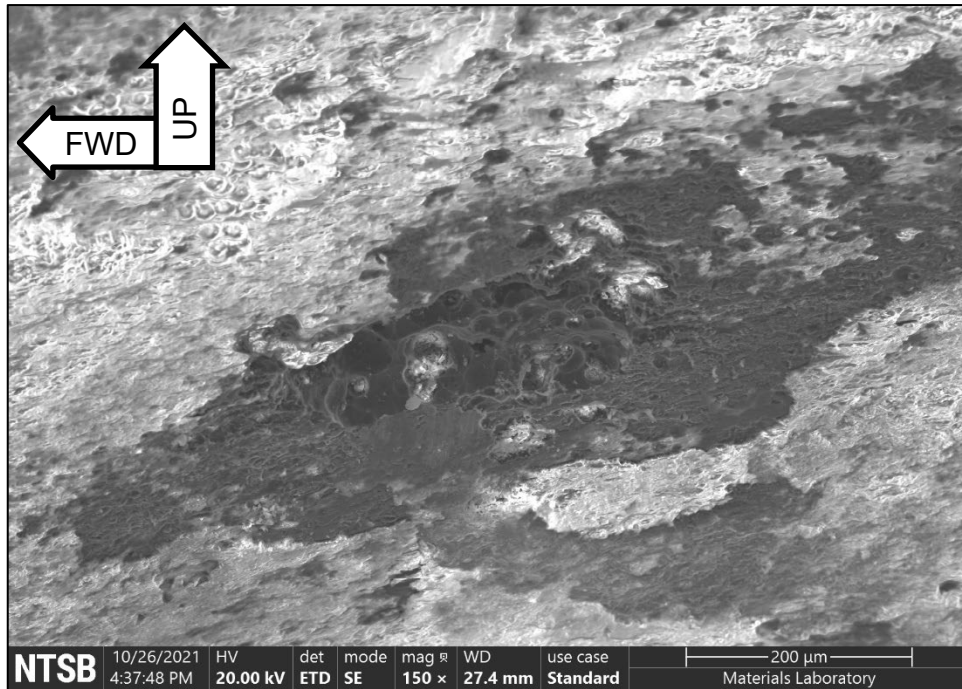


Figure A5. SEM images of the pit in the outboard side of hole LC-1.

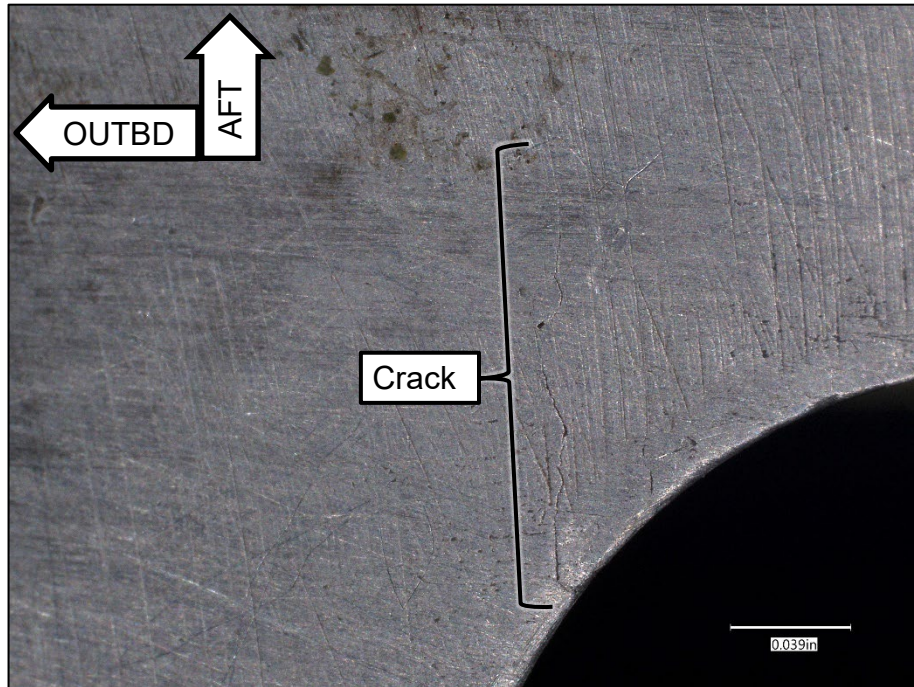


Figure A6. Optical image of the lower surface showing a crack at the outboard aft quadrant of hole LD-1.

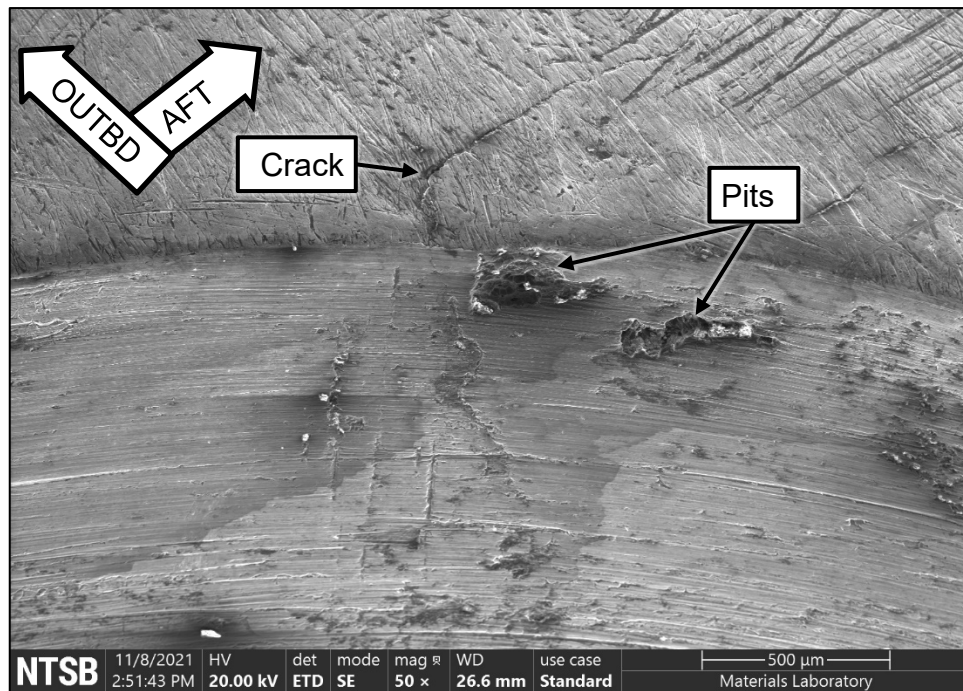


Figure A7. SEM image of the lower corner of hole LD-1 showing a crack and corrosion pits at the outboard aft quadrant.

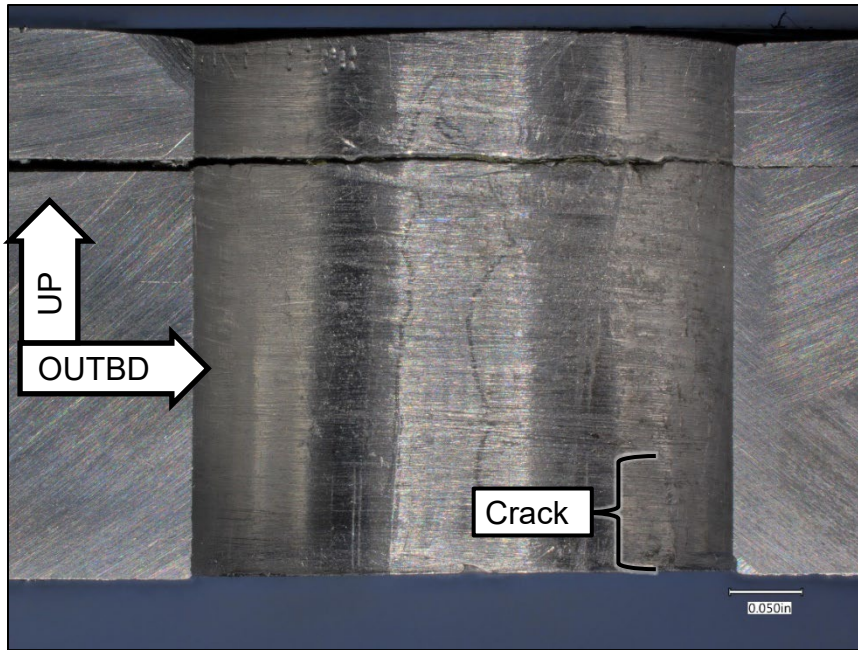


Figure A8. Optical image of the aft side of the hole LD-1 bore showing a crack at the outboard aft quadrant of hole LD-1.



Figure A9. Inboard side of the crack after opening and acetate-tape cleaning.

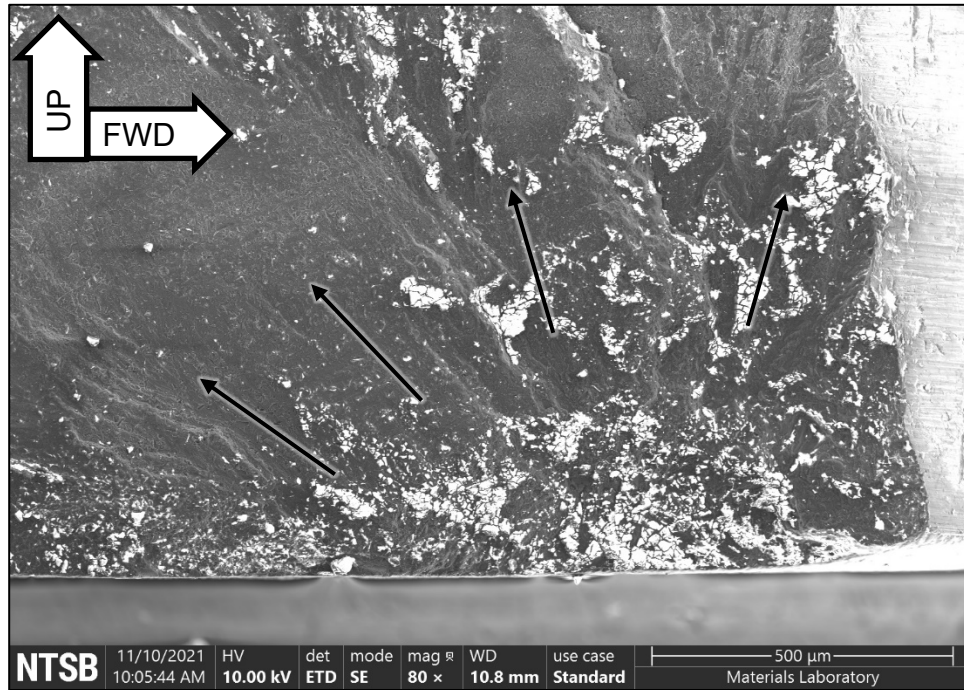


Figure A10. SEM image of the crack origin area after acetate-tape cleaning.

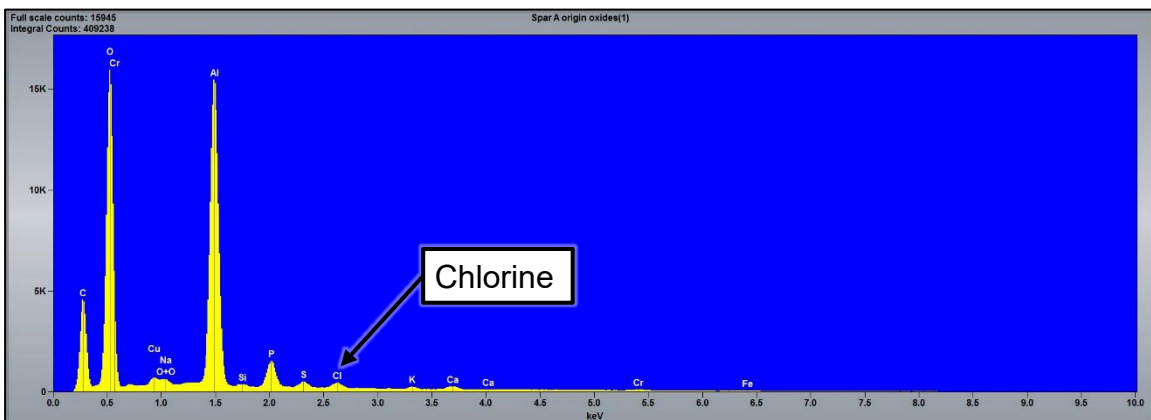


Figure A11. EDS spectrum of oxides and deposits near the origin on the acetate-tape cleaned surface (accelerating voltage = 10 kV).

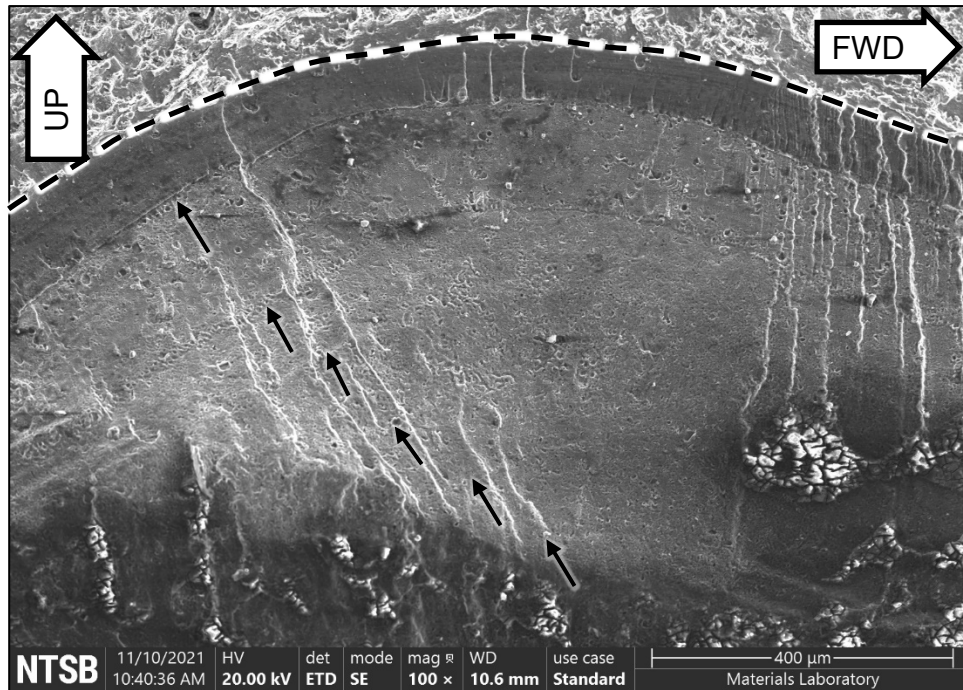


Figure A12. SEM image of the crack boundary after acetate-tape cleaning. Unlabeled arrows indicate relatively prominent crack arrest lines.

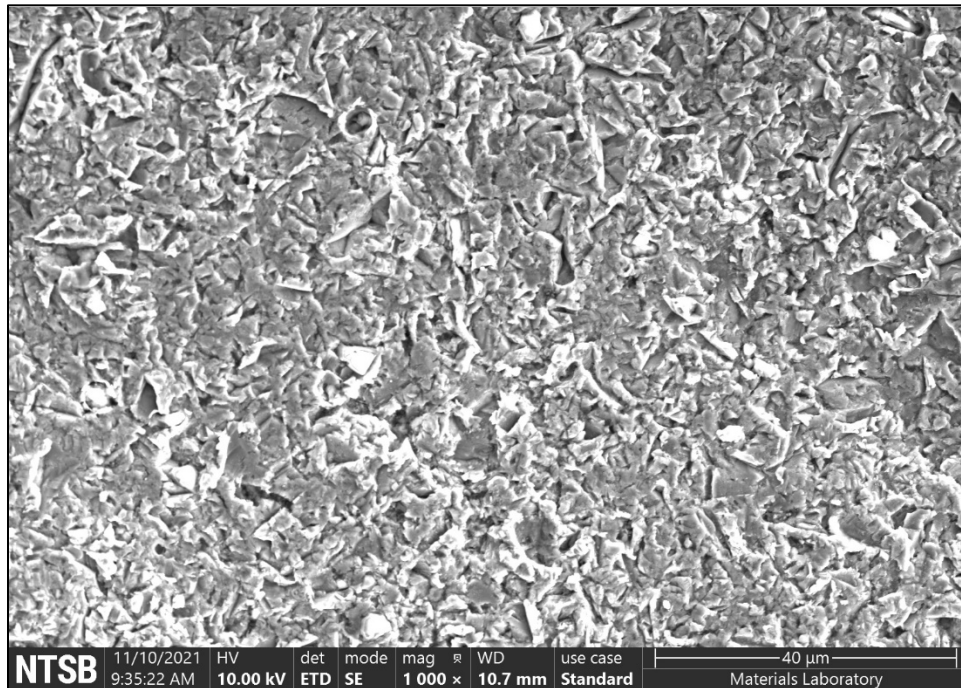


Figure A13. SEM image of fracture surface damage as observed across most of the fatigue region.

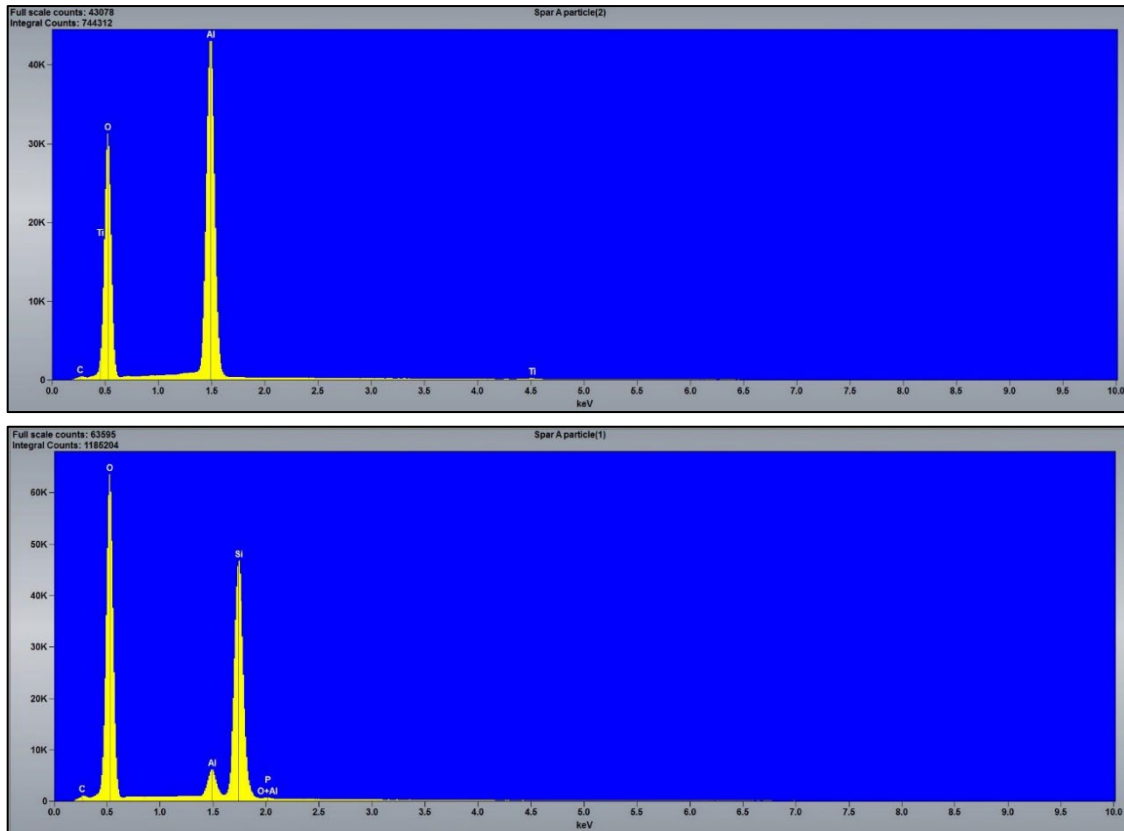


Figure A14. EDS spectra of nonconductive faceted particles observed embedded in the fracture surface (accelerating voltage = 10 kV).



Figure A15. Optical image of the fracture surface after oxide removal.

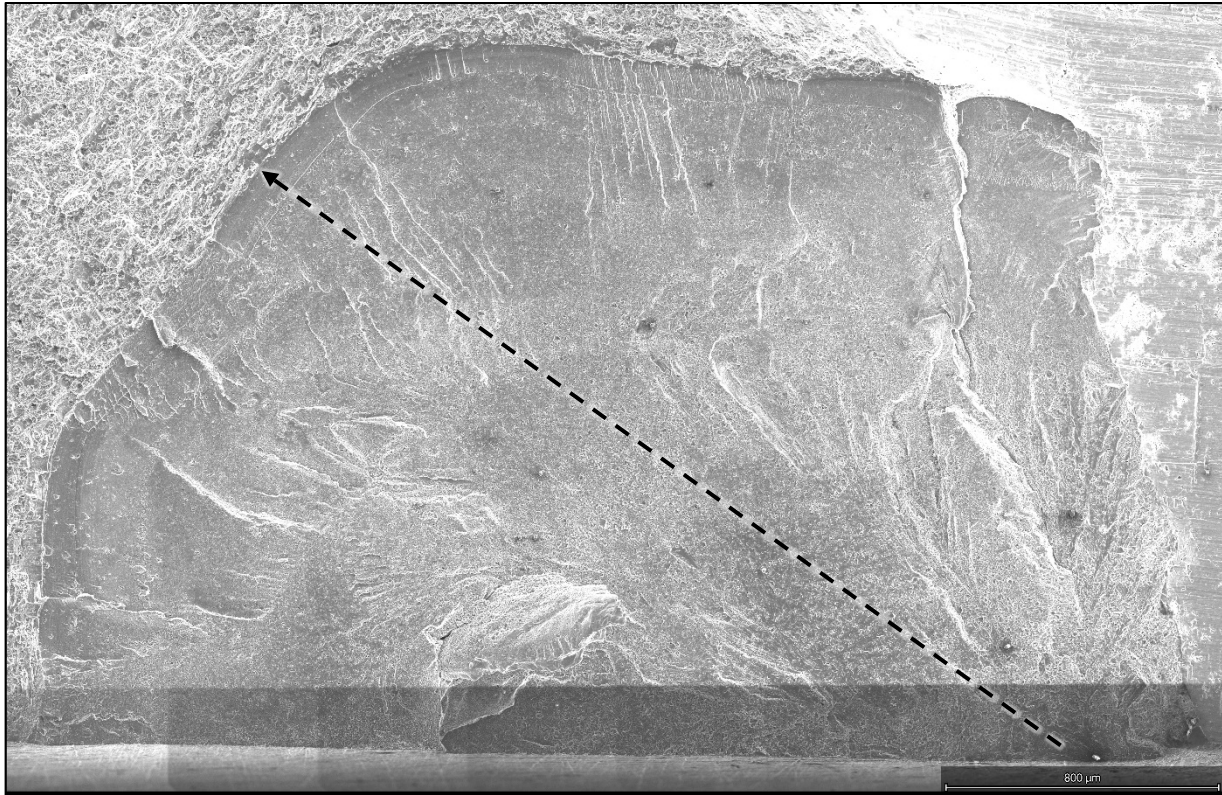


Figure A16. Montage of SEM images showing the fracture surface after oxide removal.

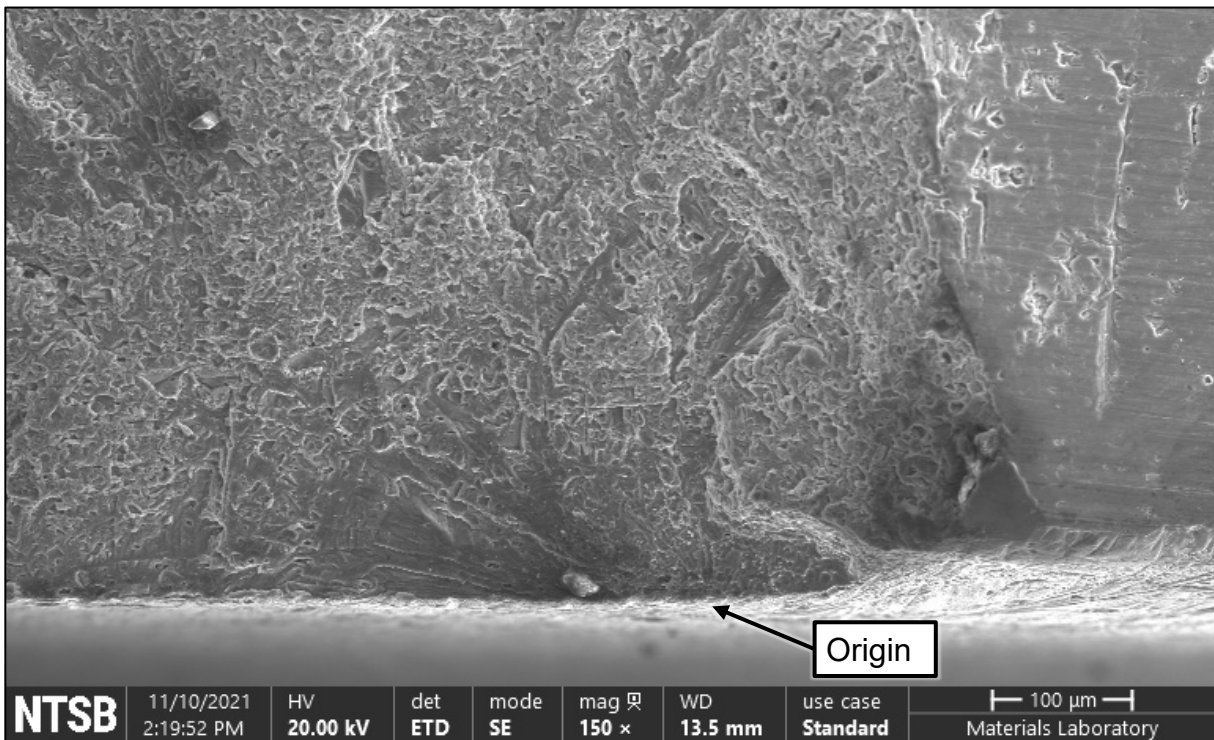


Figure A17. SEM image of the fatigue origin area after oxide removal.

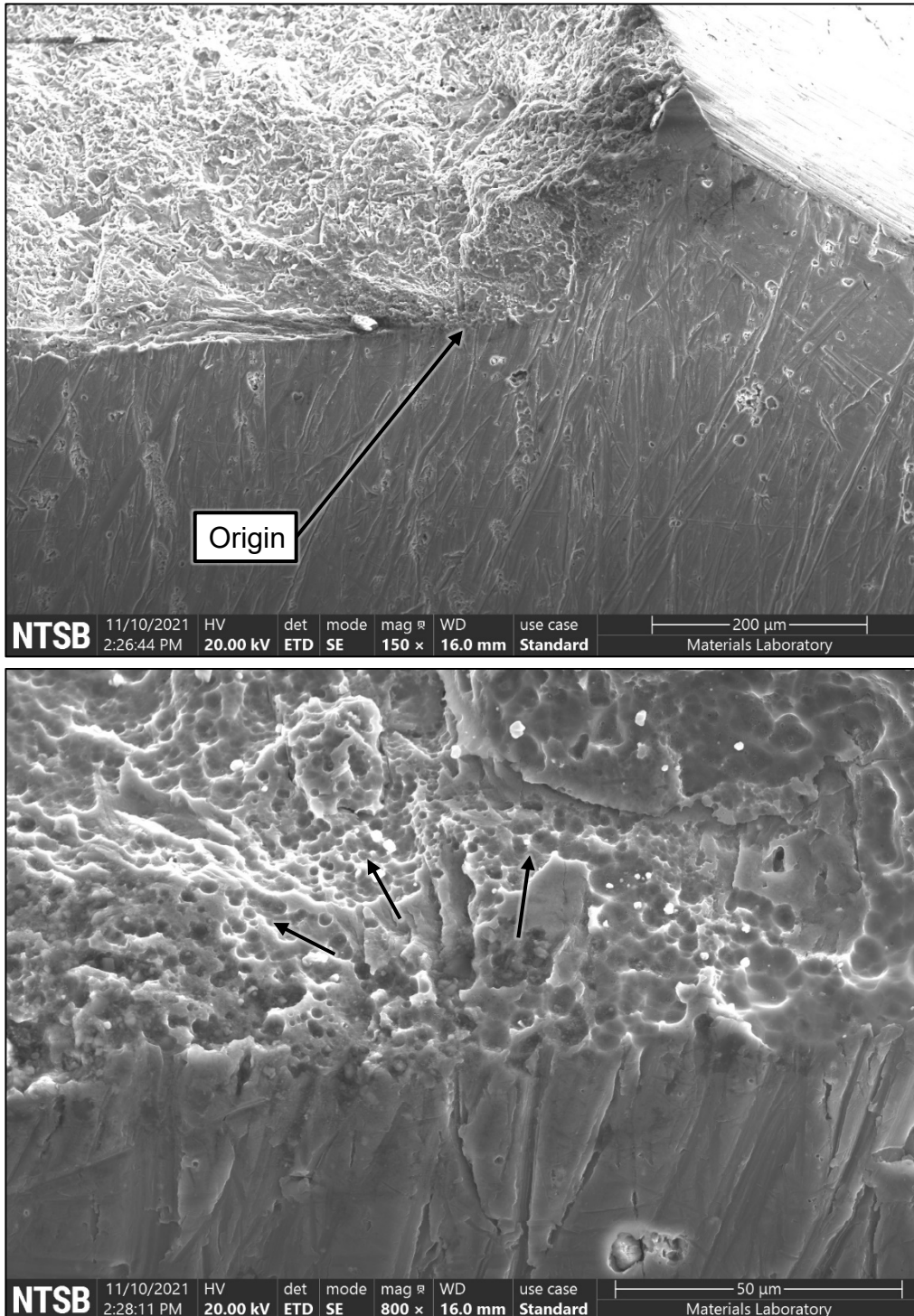


Figure A18. Oblique views of the fatigue origin after oxides removal. Unlabeled arrows in the lower image indicate fracture propagation based on apparent radial features emanating from the origin.

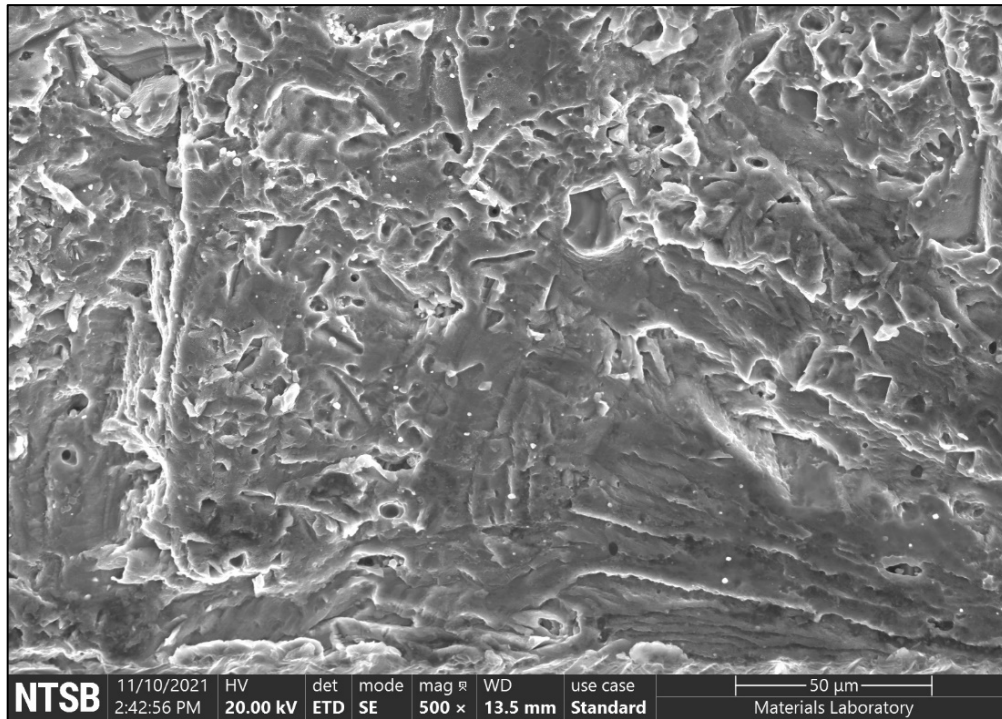


Figure A19. SEM image of fatigue features 0.0106 inch from the origin (oxides removed).

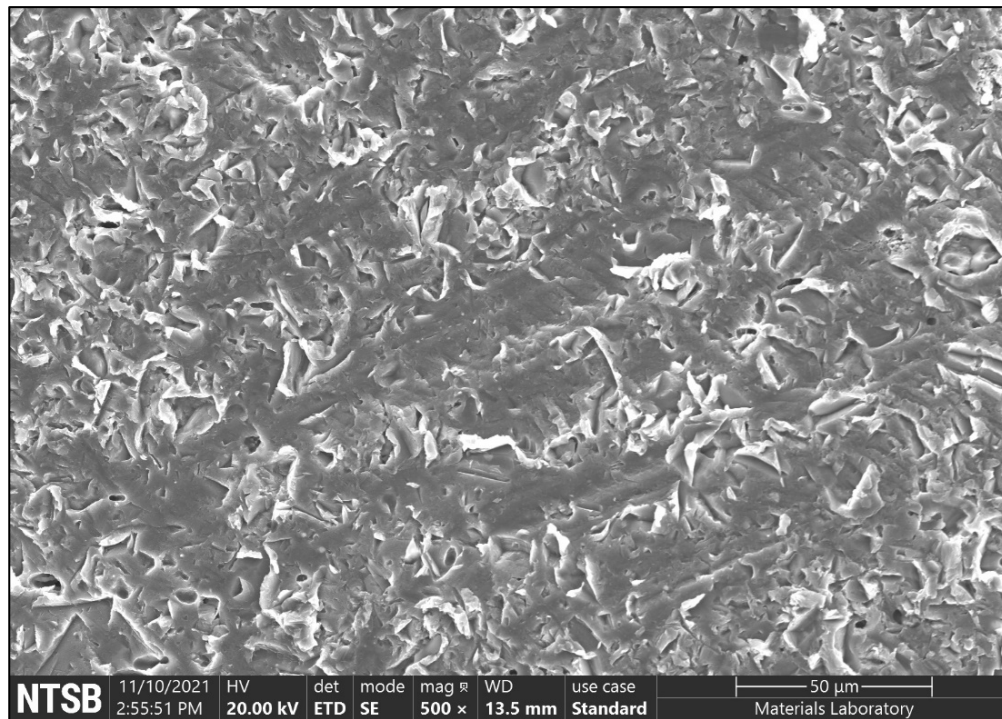


Figure A20. SEM image of fatigue features 0.0328 inch from the origin (oxides removed).

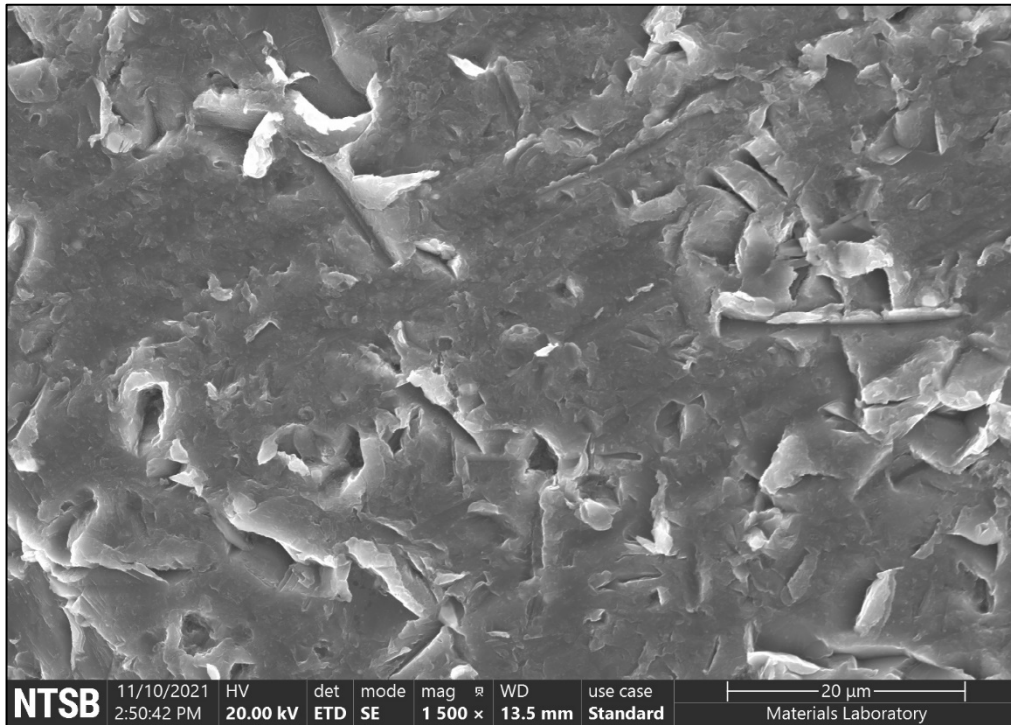


Figure A21. SEM image of fatigue features 0.0492 inch from the origin (oxides removed).

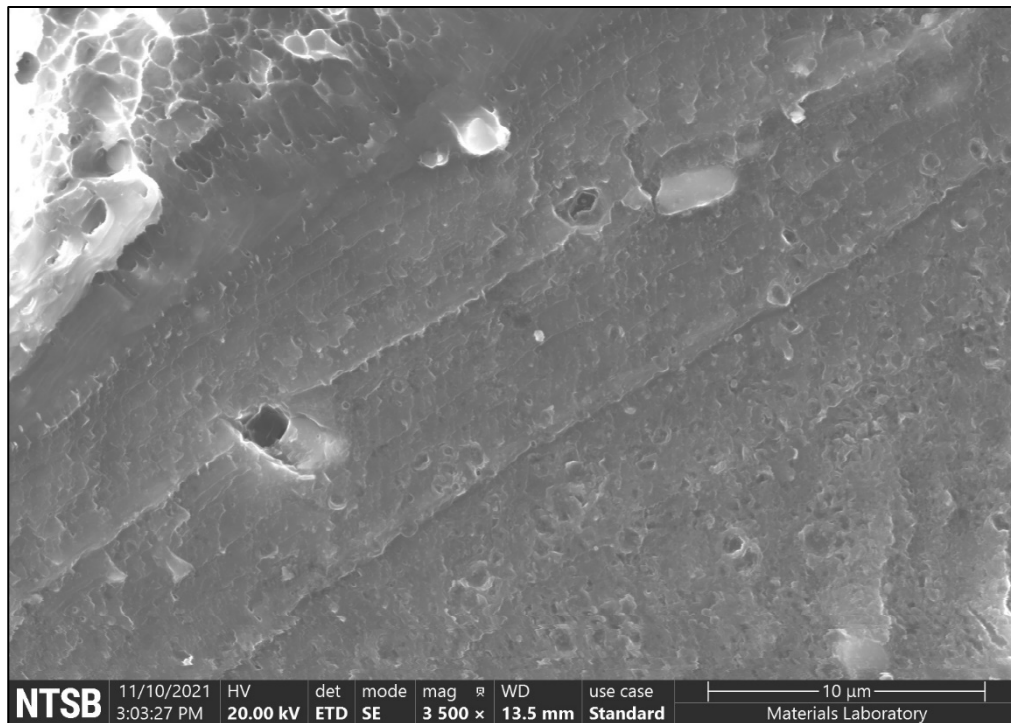


Figure A22. SEM image of fatigue features at the fatigue boundary located 0.116 inch from the origin (oxides removed).

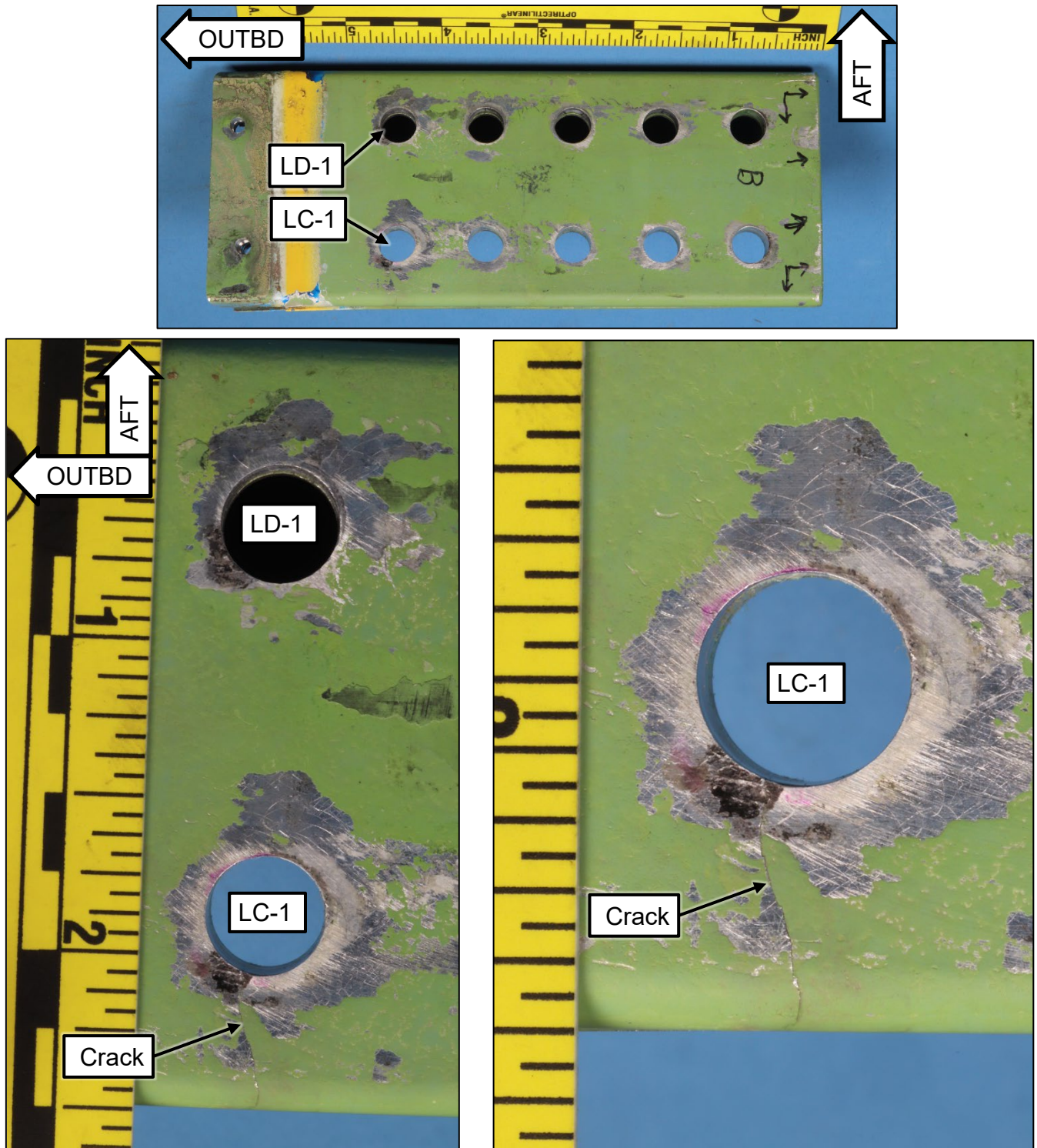


Figure B1. Spar B lower surface after wiping surfaces with acetone.

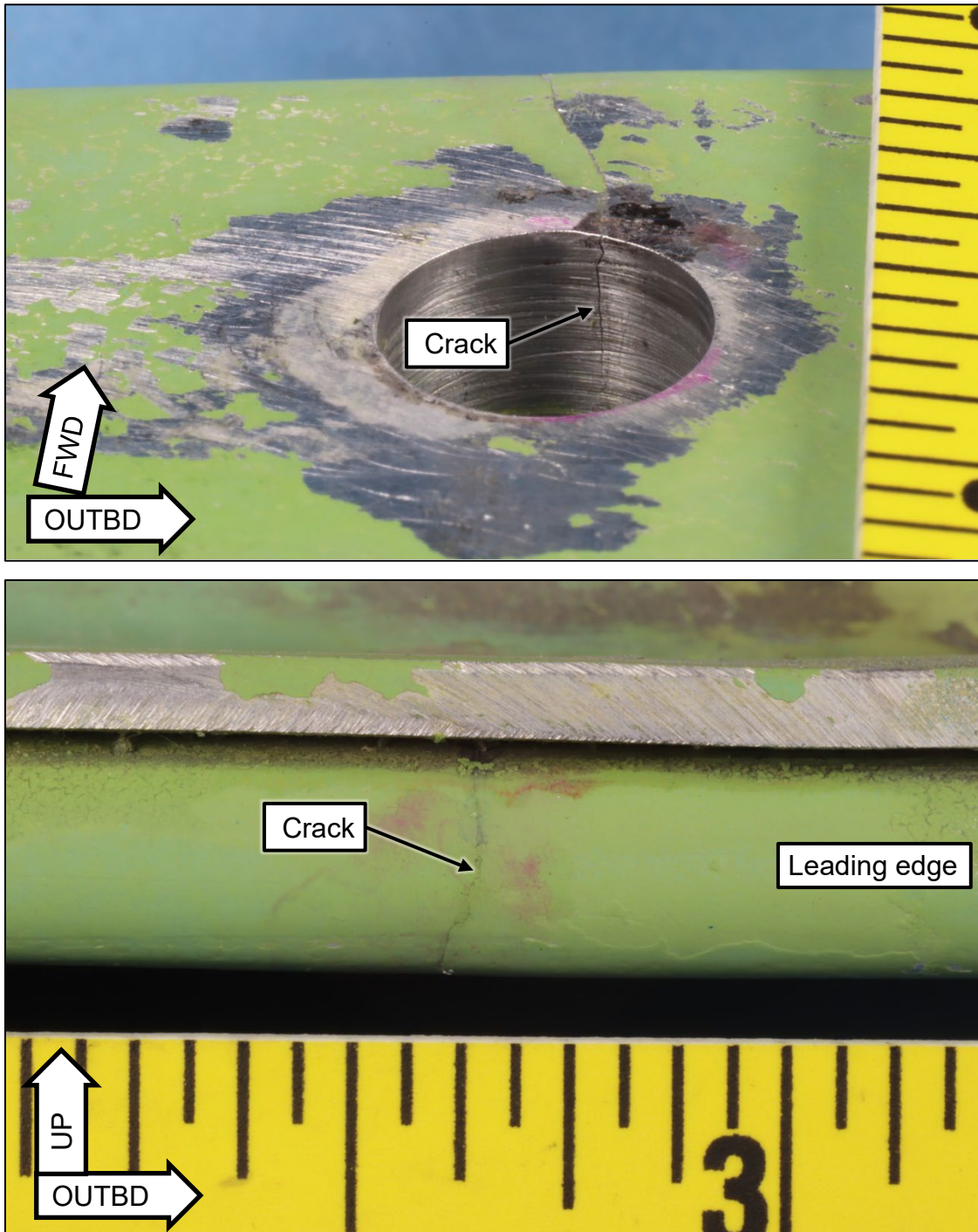


Figure B2. Crack intersecting hole LC-1 and leading edge.

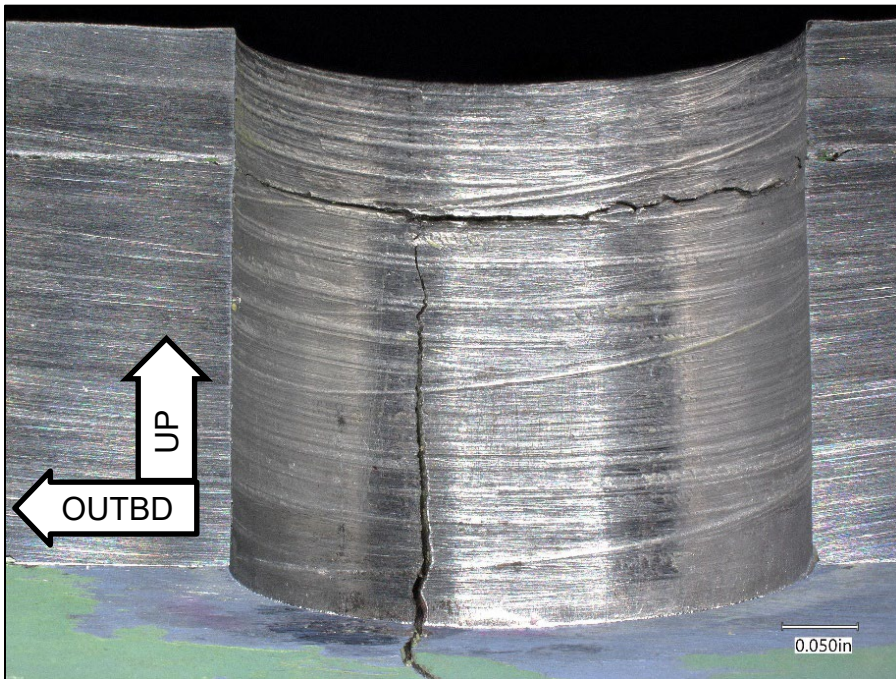


Figure B3. Forward side of hole LC-1 after sectioning.

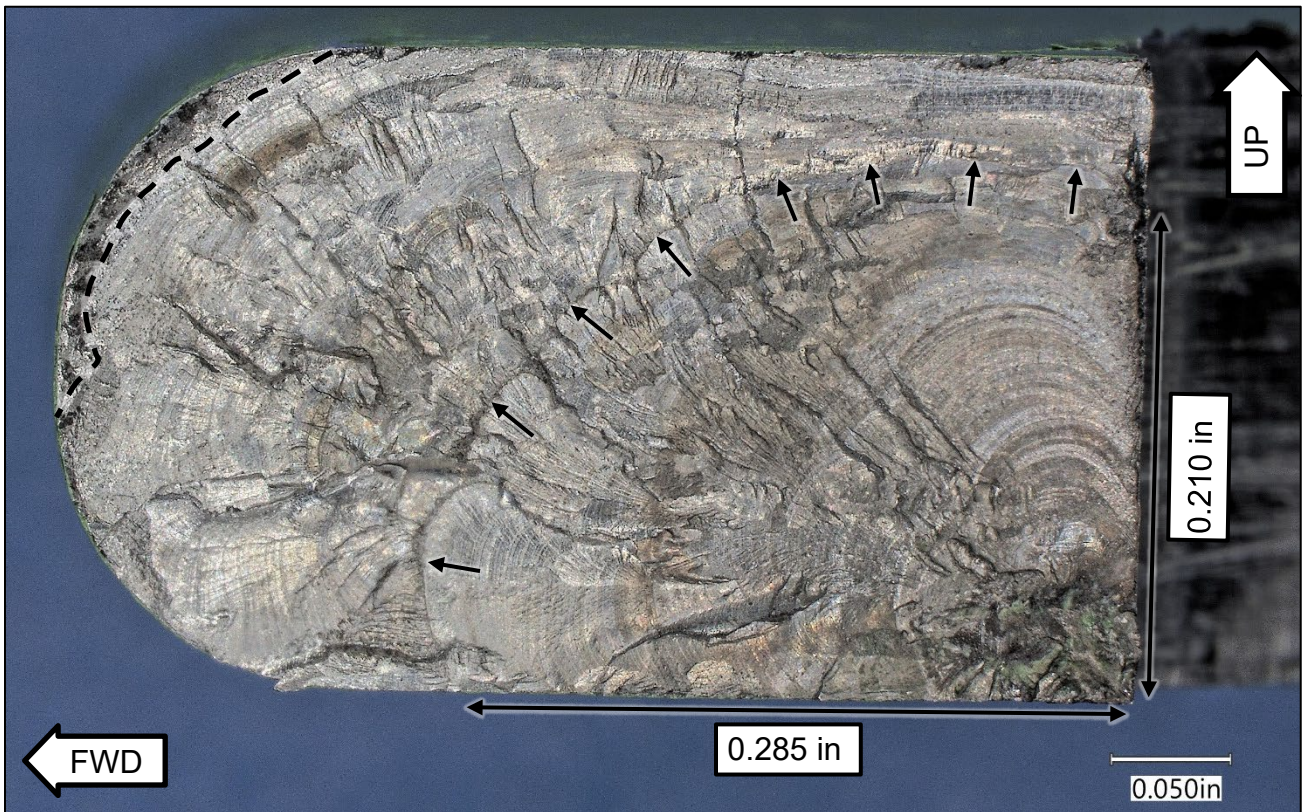


Figure B4. Inboard side of the fracture surface after cleaning with acetate tape and acetone. A dashed line indicates the fatigue boundary, and unlabeled arrows indicate a relatively strong crack arrest mark.

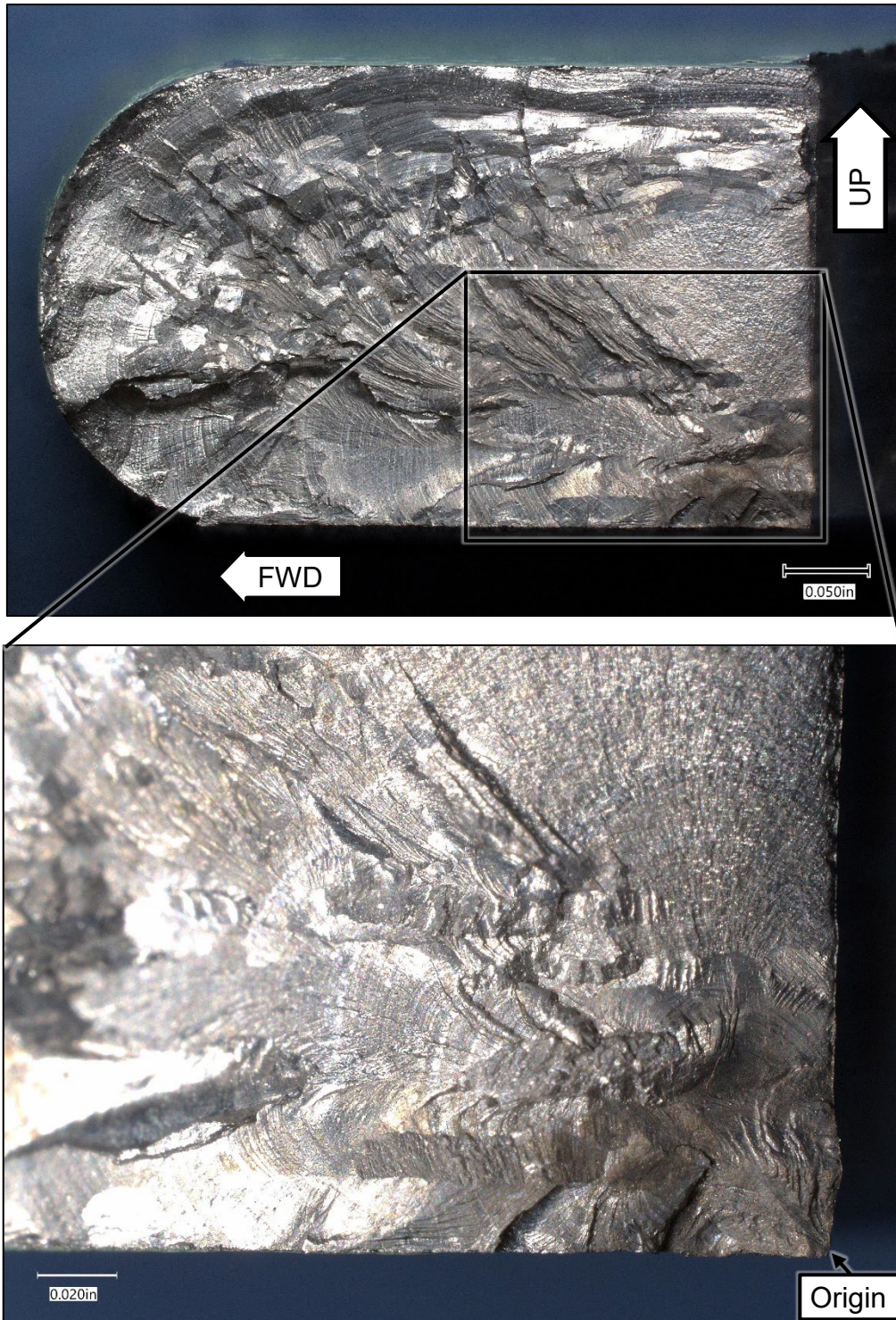


Figure B5. Inboard side of the fracture surface after oxide removal.

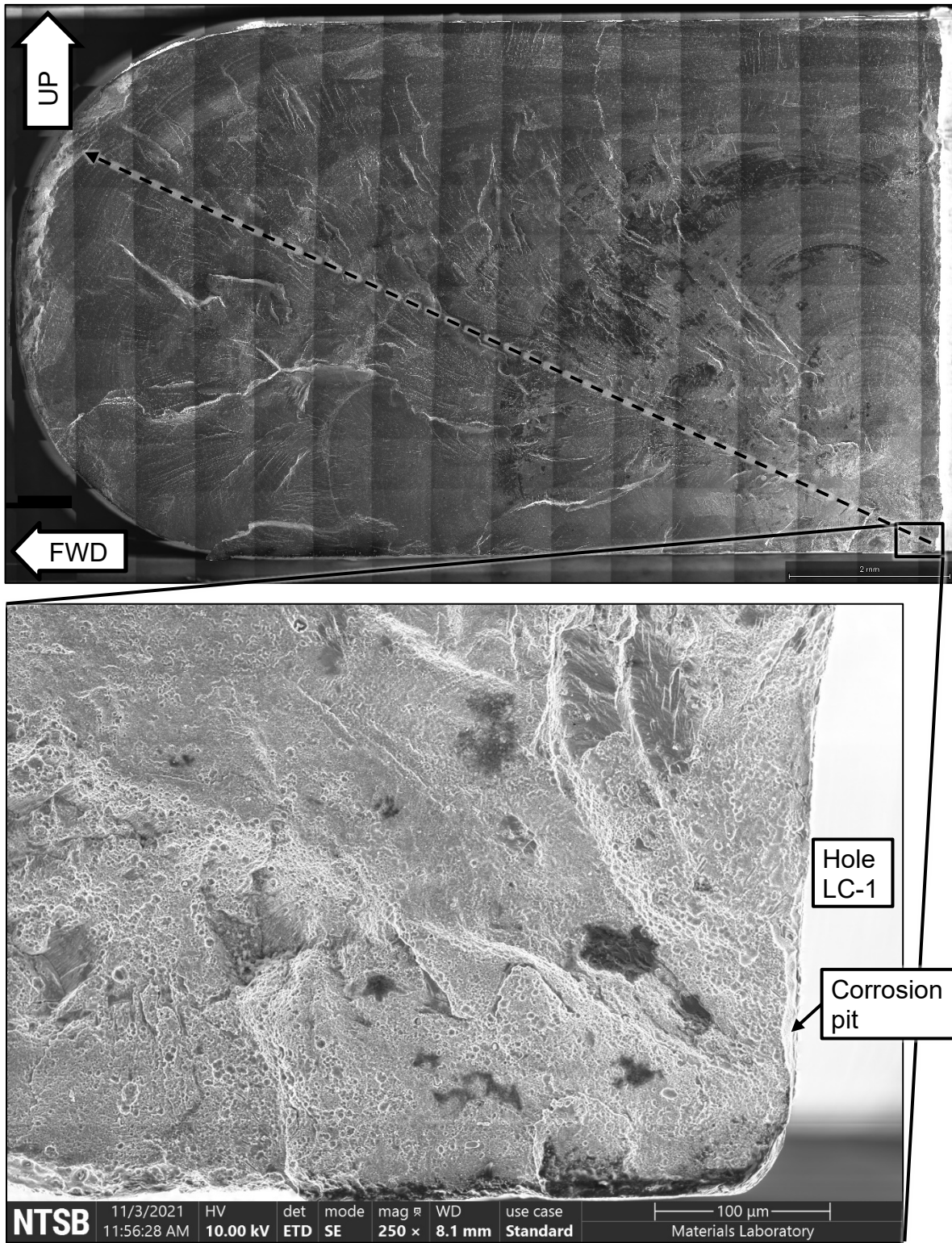


Figure B6. SEM images of the fracture surface after oxide removal.

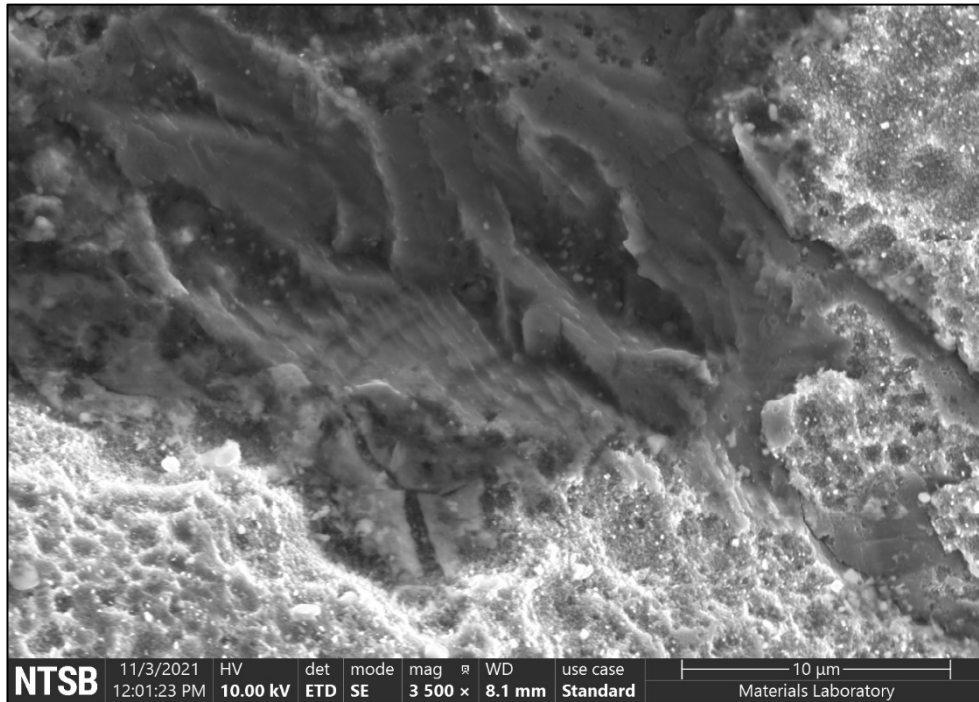


Figure B7. Fatigue features 0.0024 inch from the origin (oxides removed).

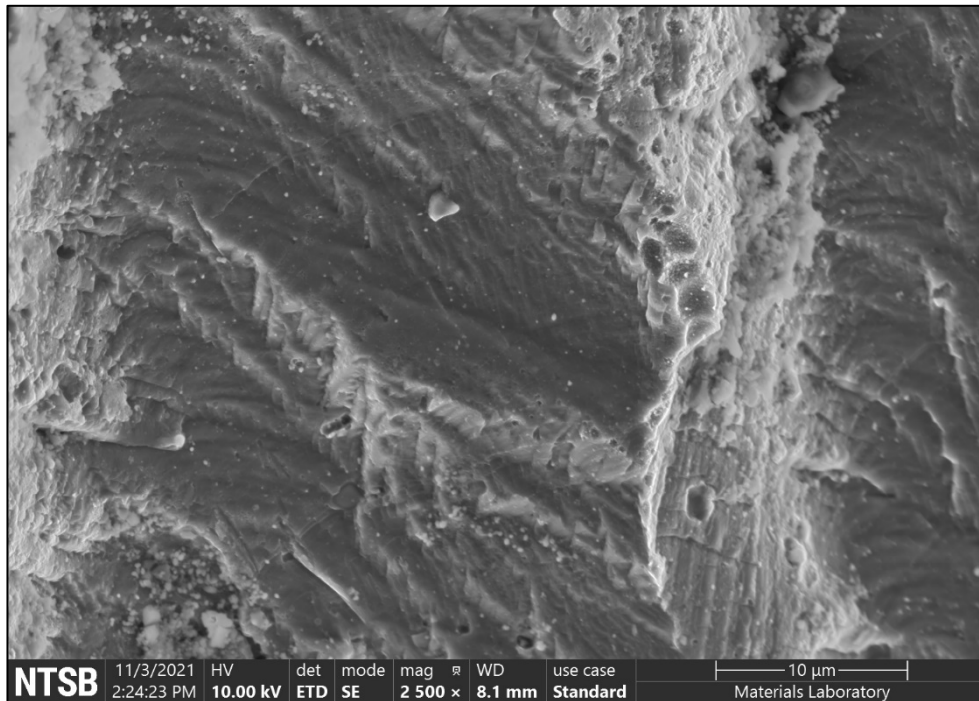


Figure B8. Fatigue features 0.0089 inch from the origin (oxides removed).

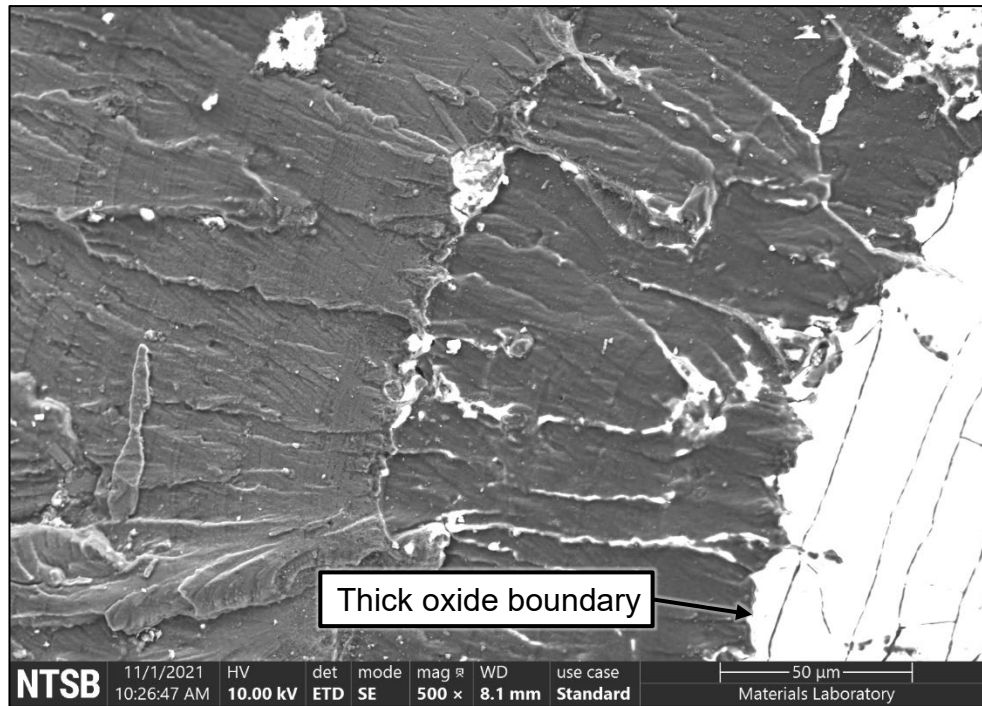


Figure B9. Fatigue features 0.114 inch from the origin (before oxide removal).

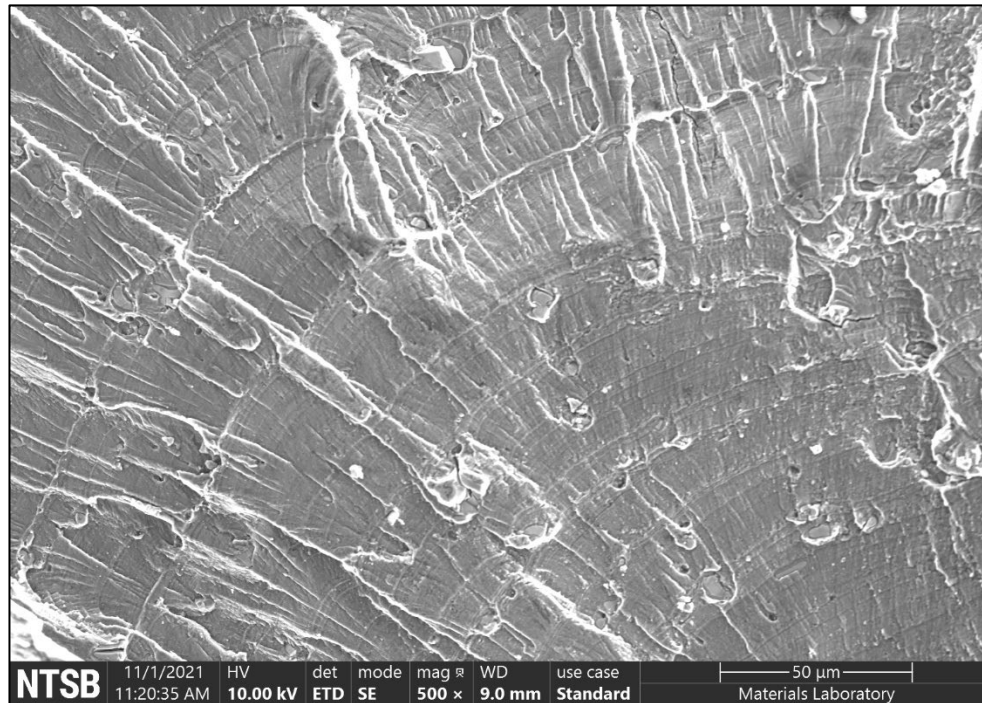


Figure B10. Fatigue features 0.274 inch from the origin (before oxide removal).

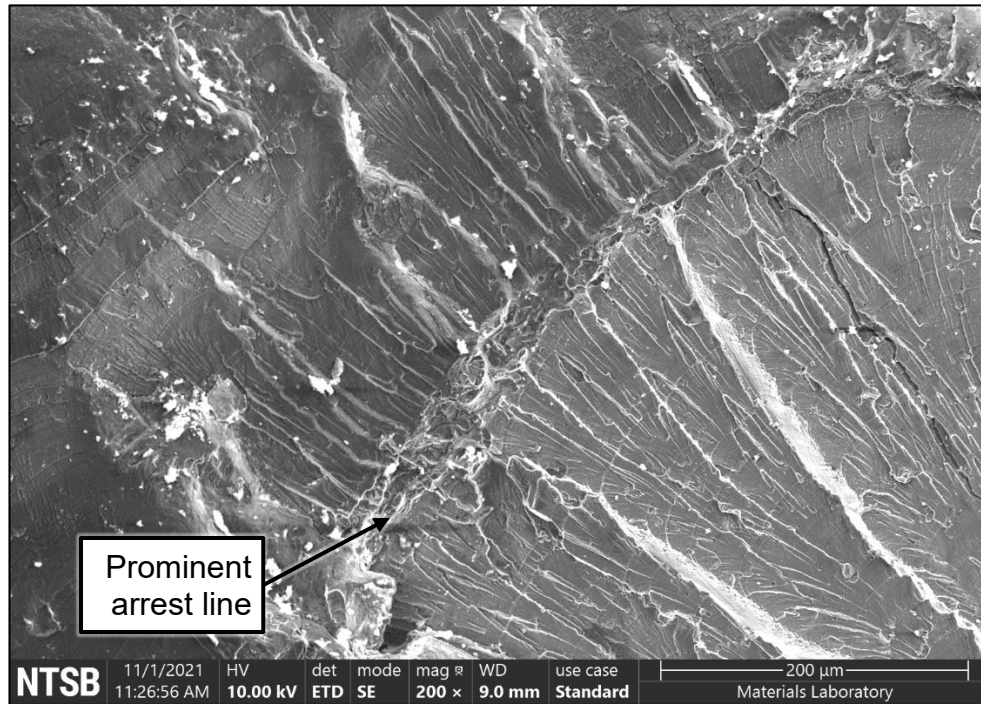


Figure B11. Fatigue features 0.295 inch from the origin showing the prominent crack arrest line (before oxide removal).

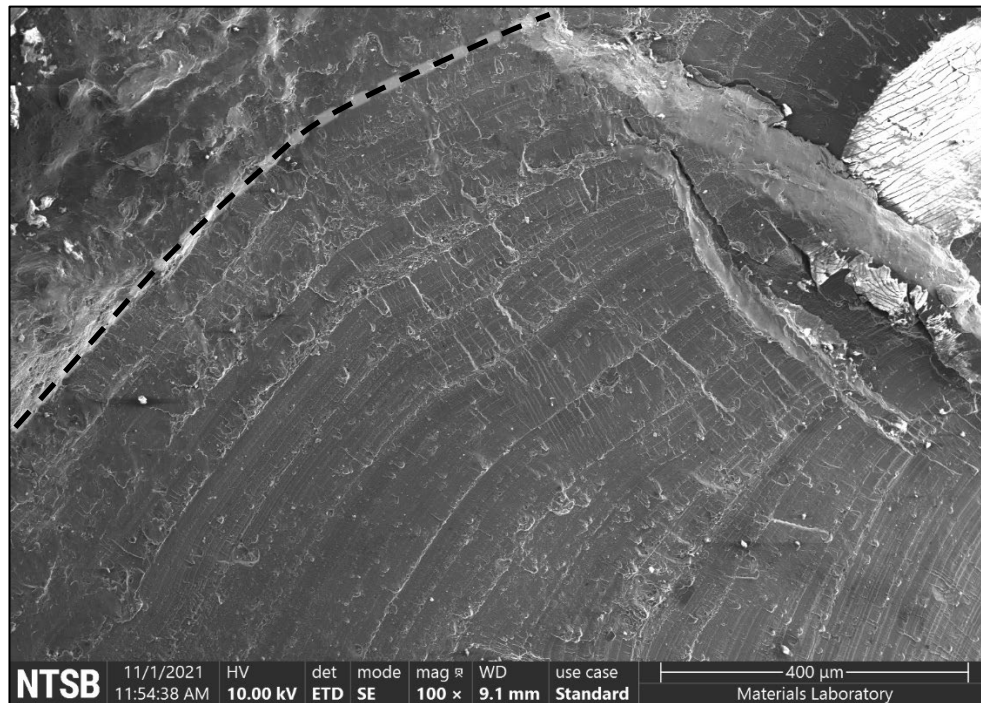


Figure B12. Fatigue features at the fatigue boundary (before oxide removal).

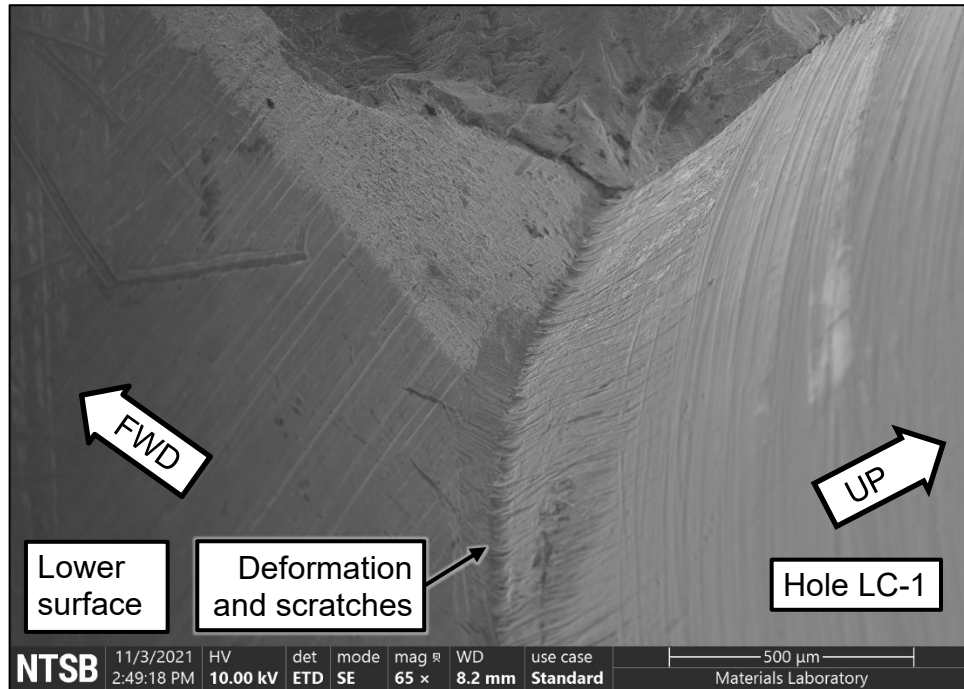


Figure B13. Deformed and scratched forward lower corner of hole LC-1 (after oxide removal).

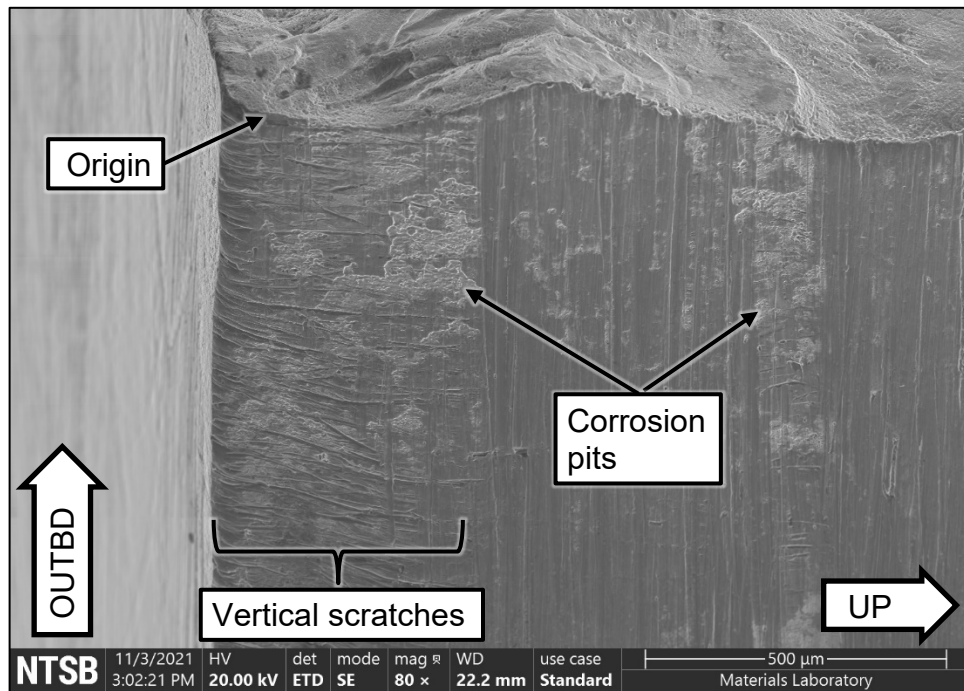


Figure B14. Hole LC-1 surface adjacent to the fatigue origin showing corrosion pits and vertical scratches (after oxide removal).

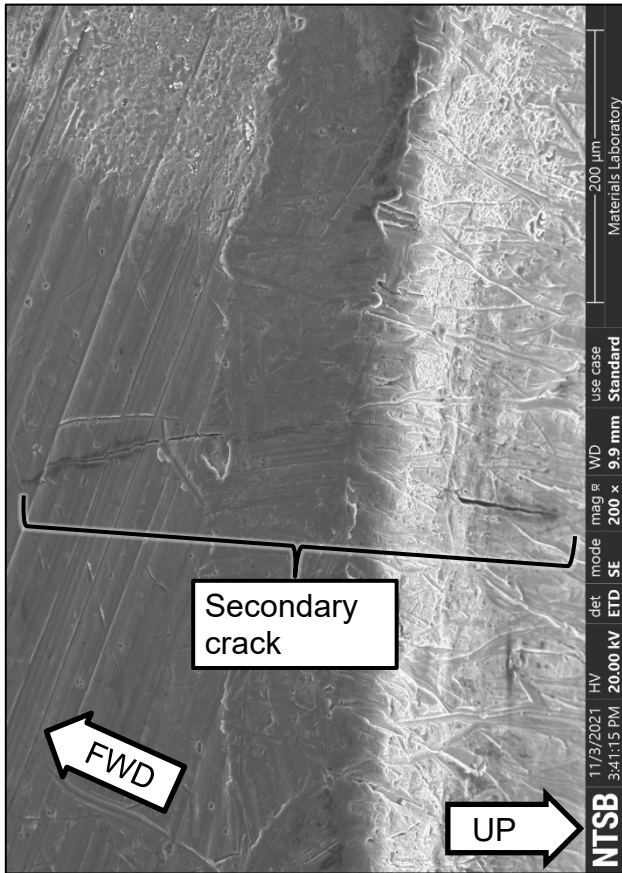


Figure B15. Secondary crack at the hole LC-1 lower forward corner (after oxide removal).

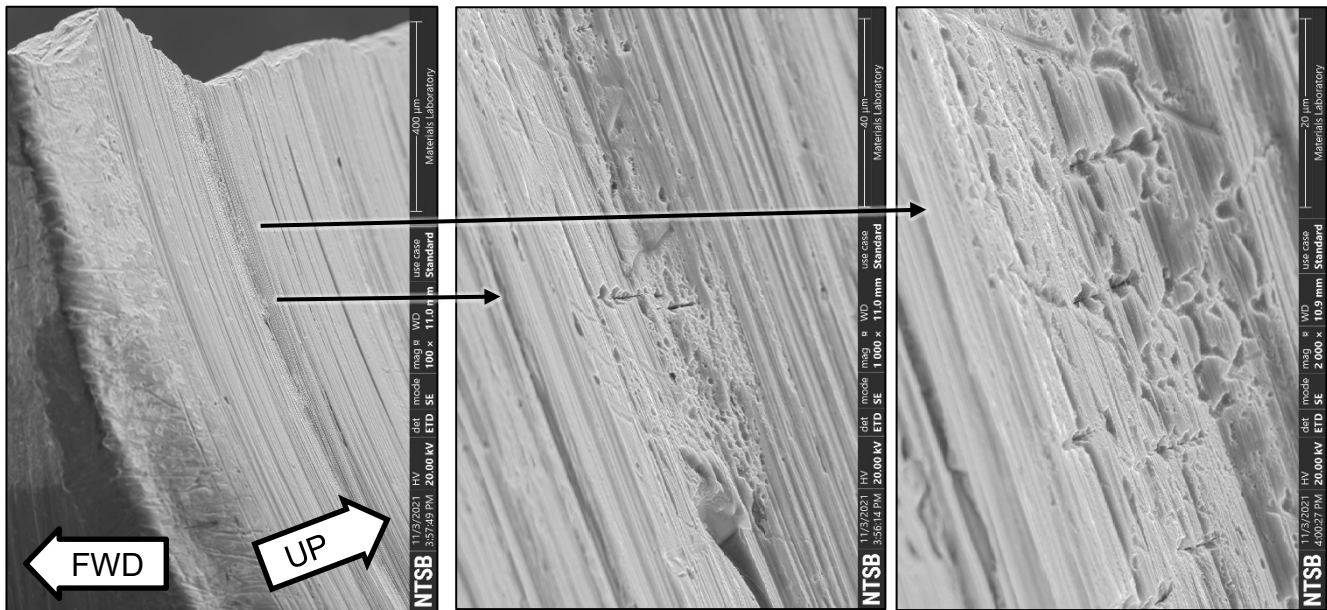


Figure B16. Secondary cracks at corrosion pits in the hole LC-1 bore (after oxide removal).

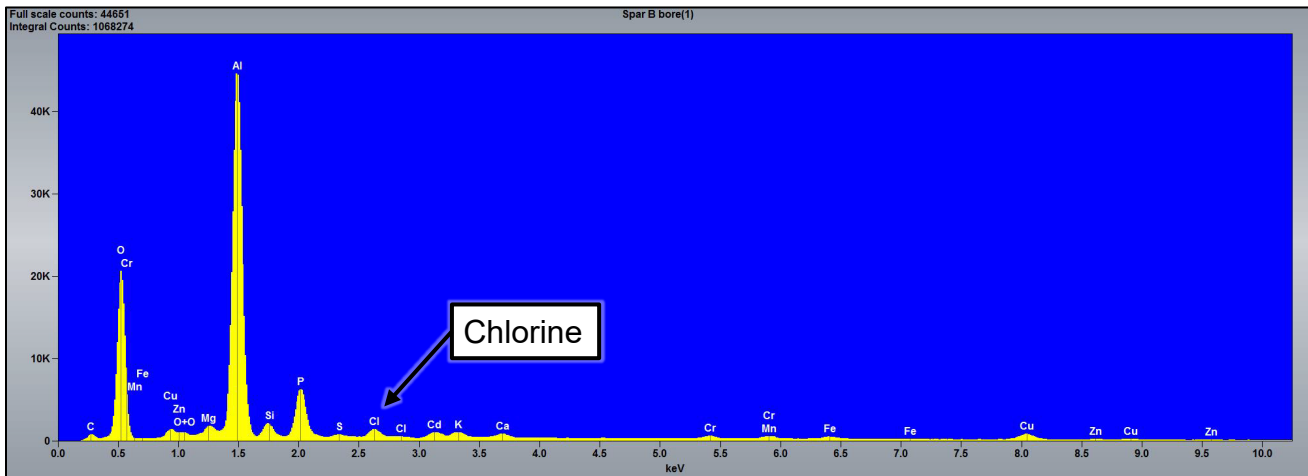
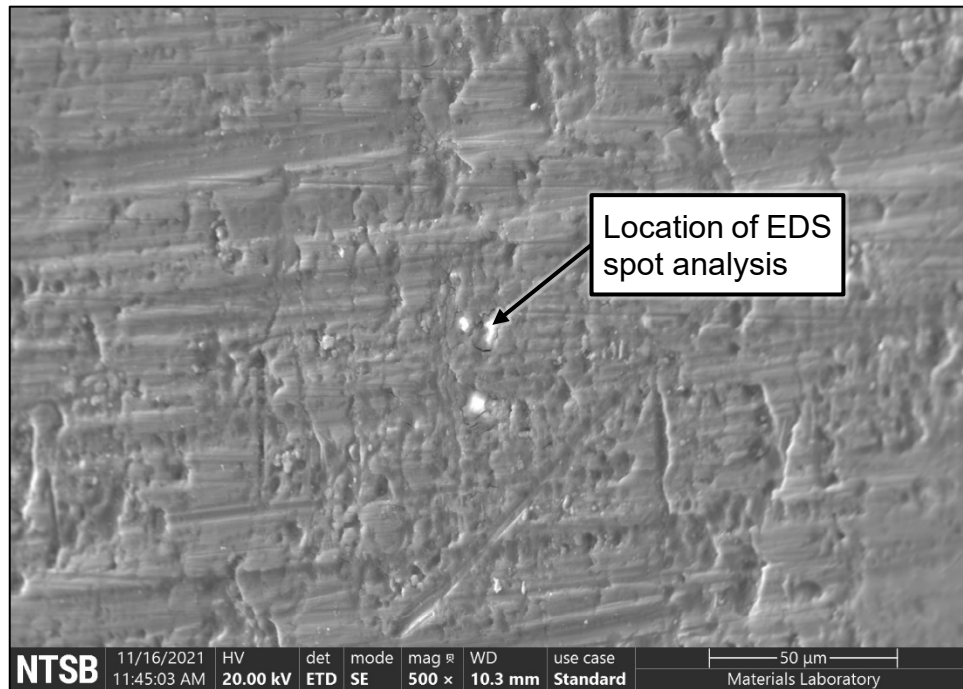


Figure B17. SEM image of the hole LC-1 bore as cleaned with acetone (upper image). The oxide at the location indicated was analyzed using EDS, resulting in the spectrum shown.

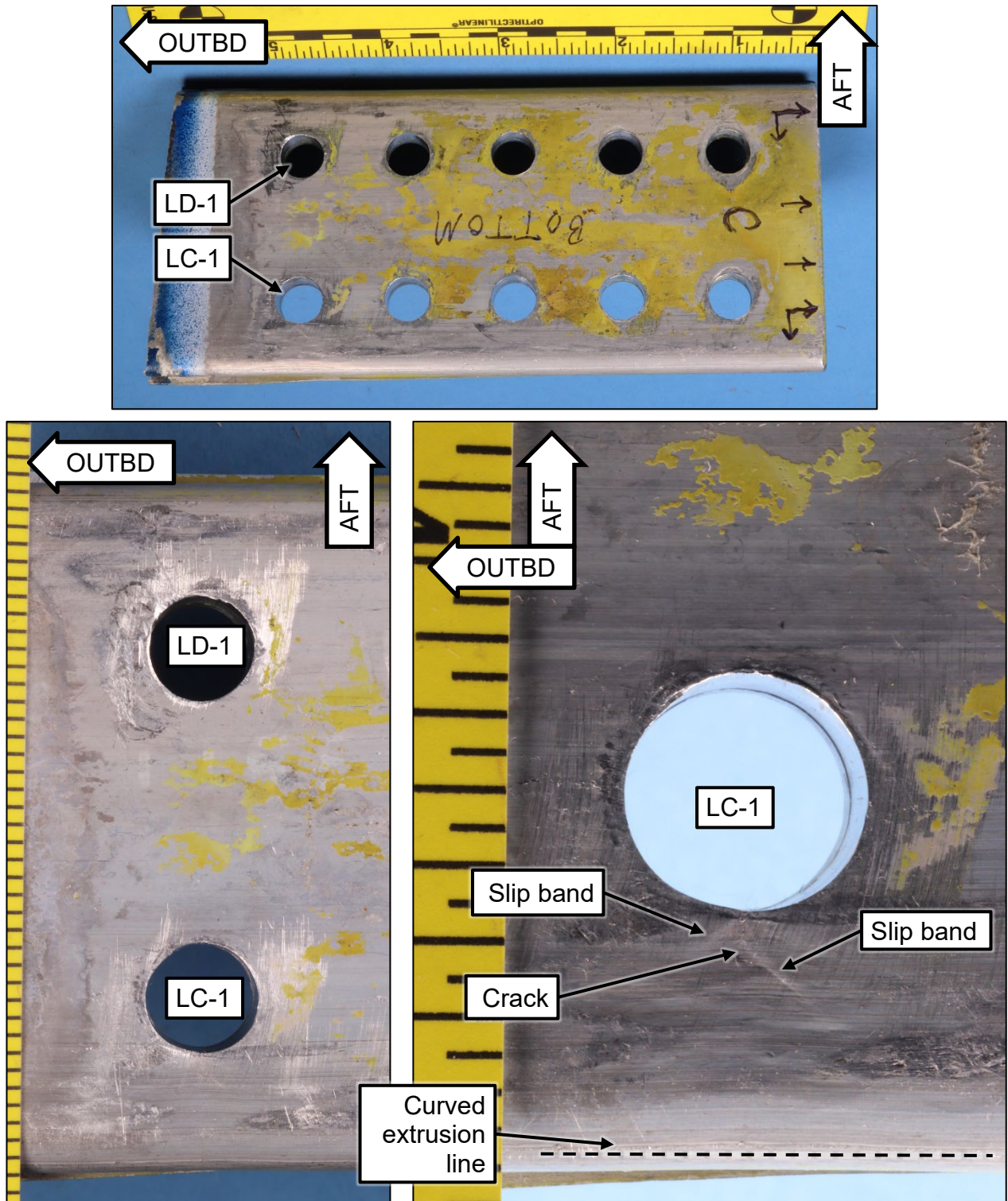


Figure C1. Spar C lower surface after wiping surfaces with acetone.

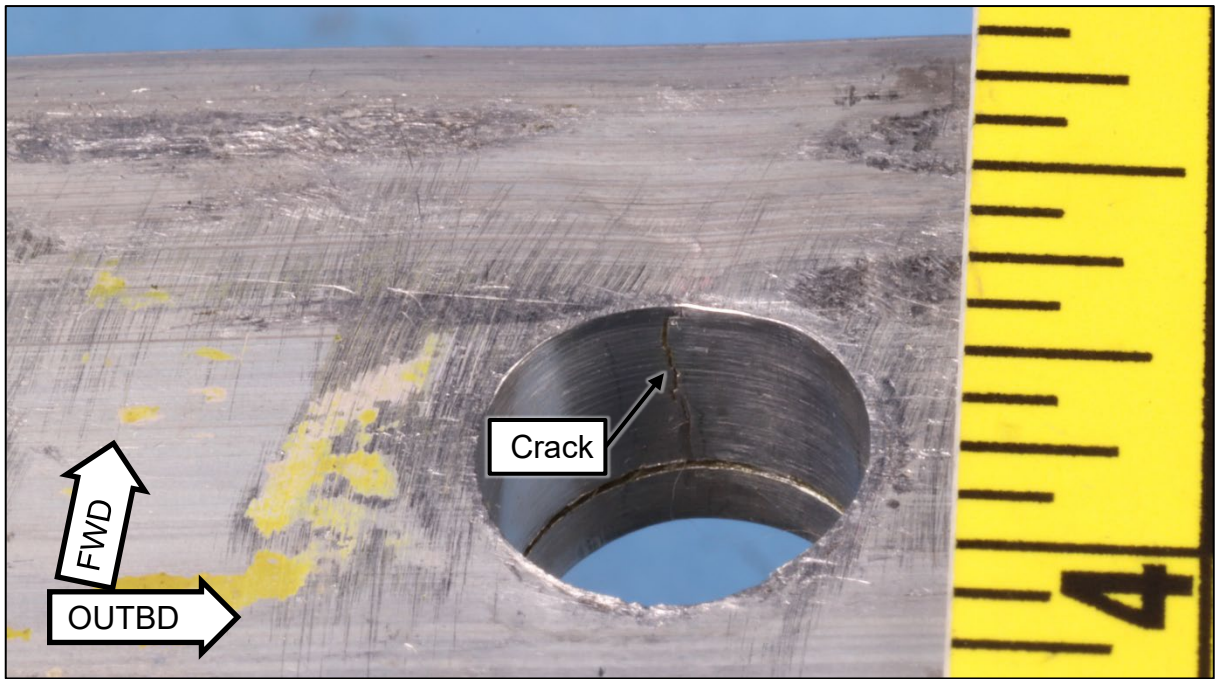


Figure C2. Crack on forward side of hole LC-1.

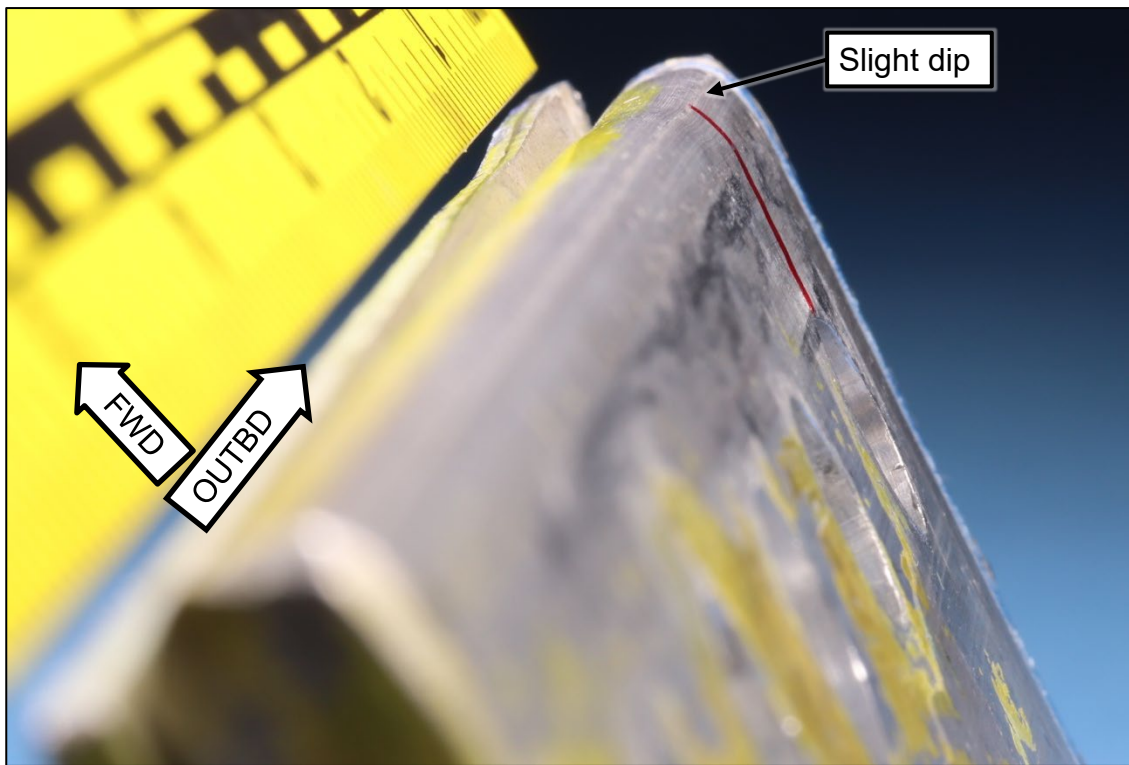


Figure C3. Deformation of the spar leading edge forward of hole LC-1.



Figure C4. The lower flange of the aft doubler was slightly bent aft of hole LD-1.

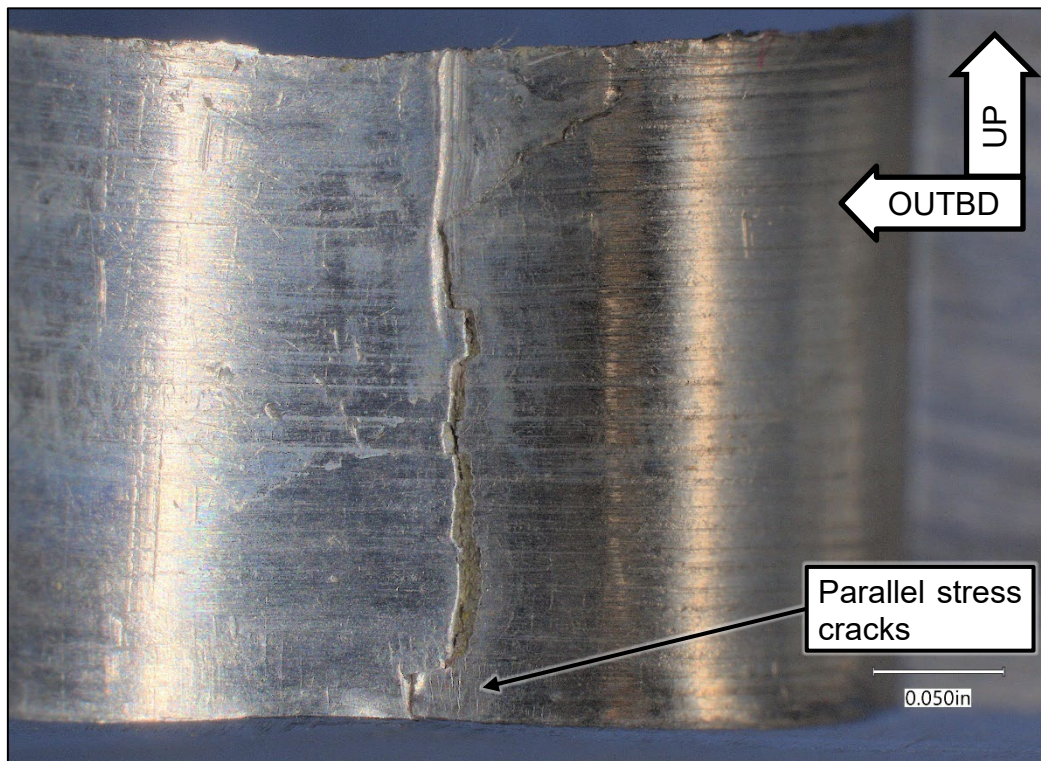


Figure C5. Forward side of hole LC-1 after sectioning showing parallel cracks consistent with stress cracks.

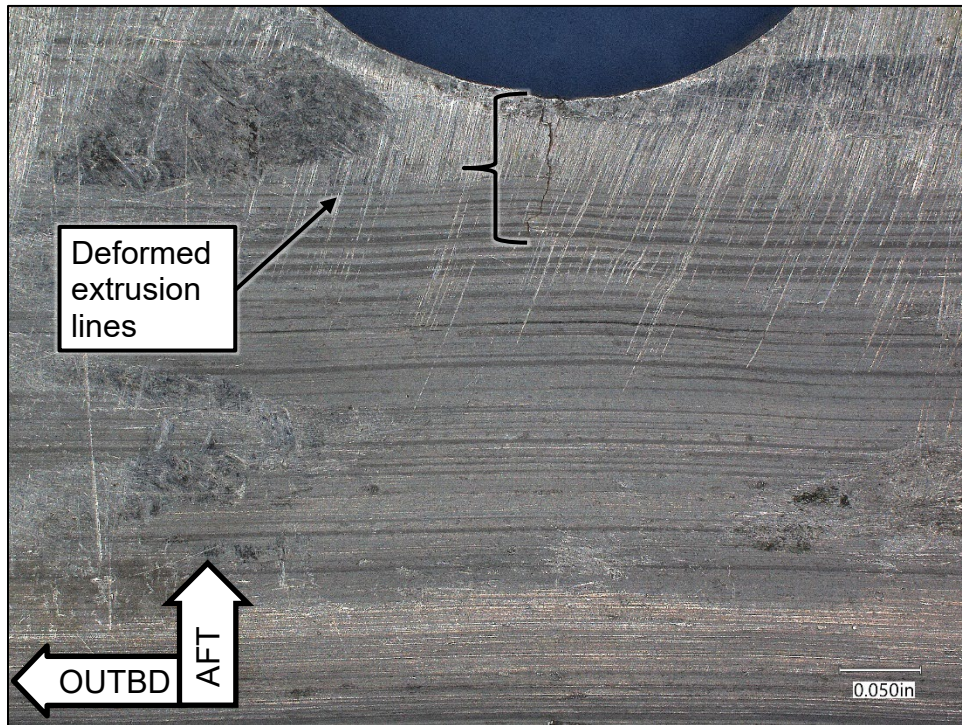


Figure C6. Lower surface forward of hole LC-1 showing the crack and deformed extrusion lines.

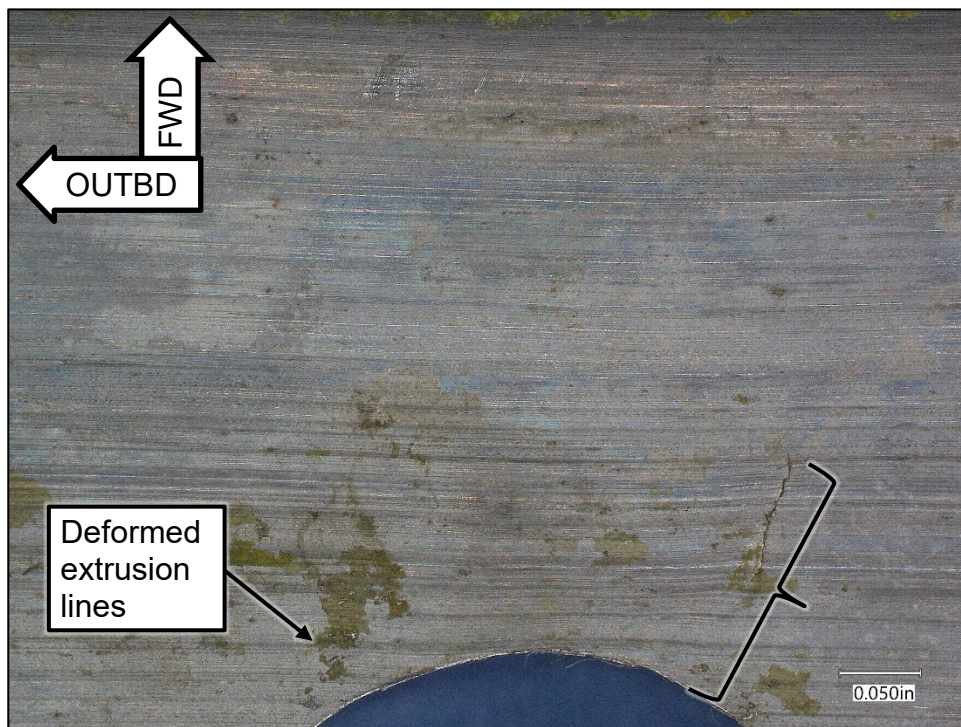


Figure C7. Upper surface forward of hole LC-1 showing the crack and deformed extrusion lines.

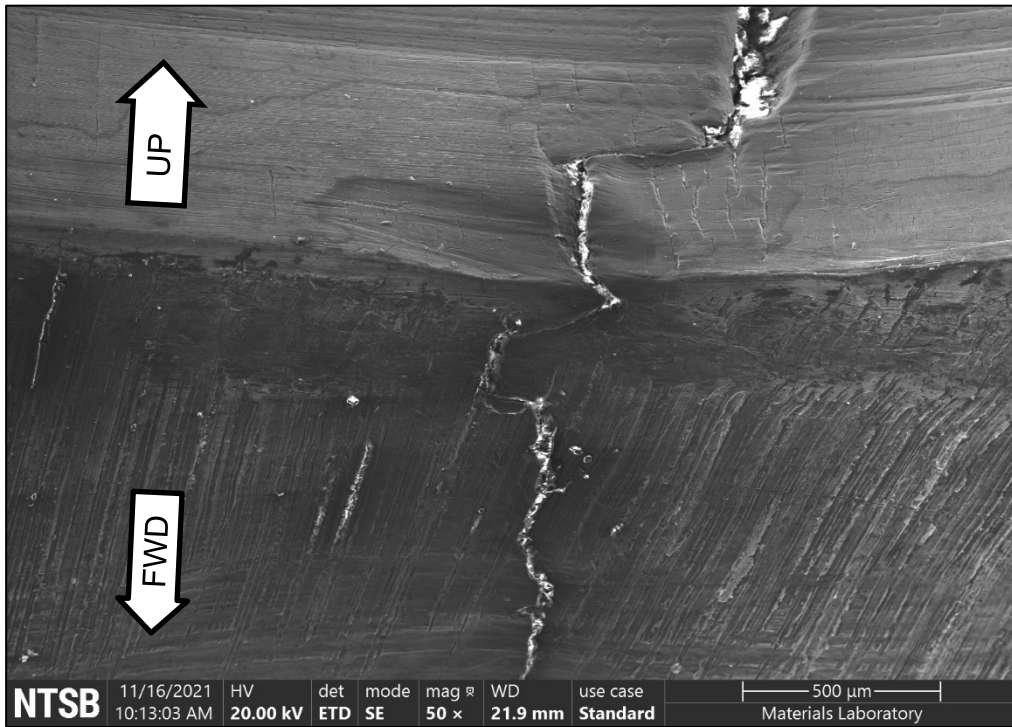


Figure C8. SEM image of the crack in an oblique view of the lower forward corner of hole LC-1.

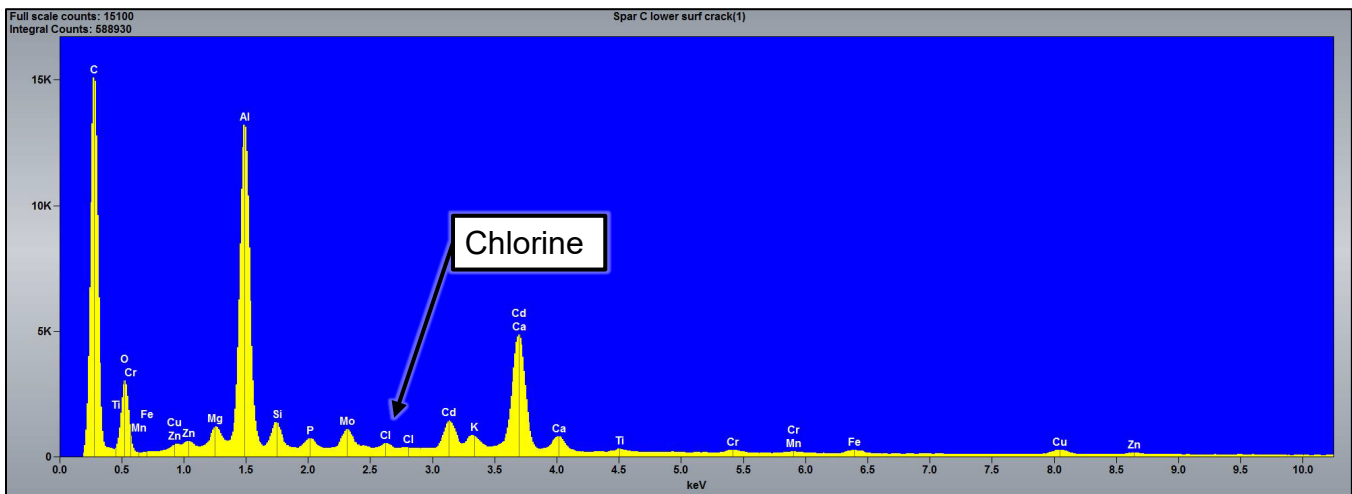


Figure C9. EDS spectrum of nonconductive material in the crack opening as analyzed at the hole LC-1 corner.

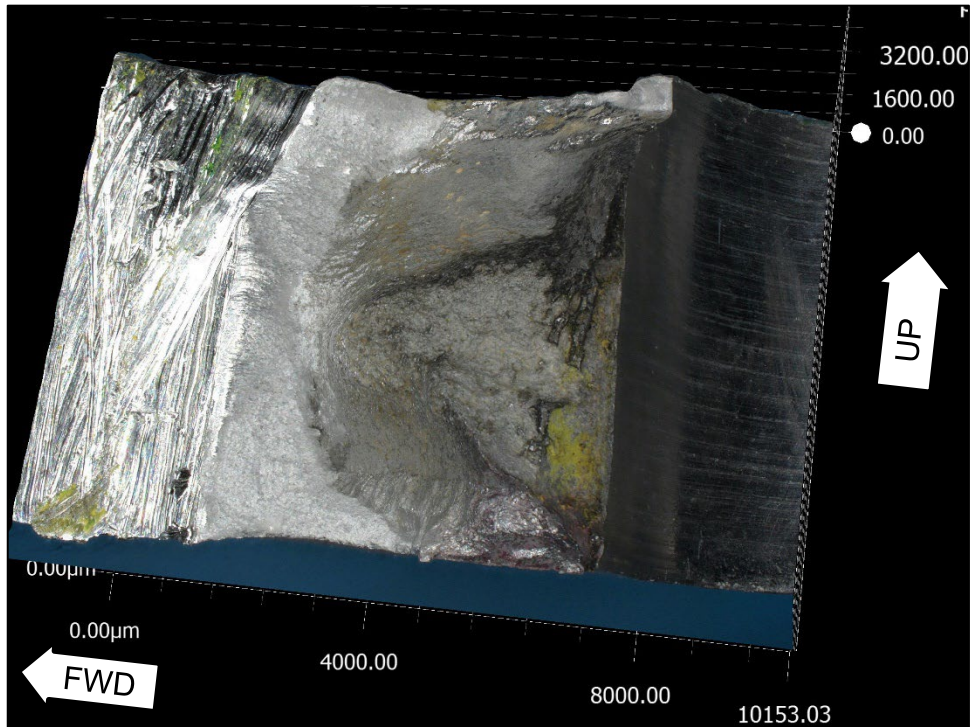


Figure C10. Three-dimensional representation of the opened crack after cleaning using acetone.

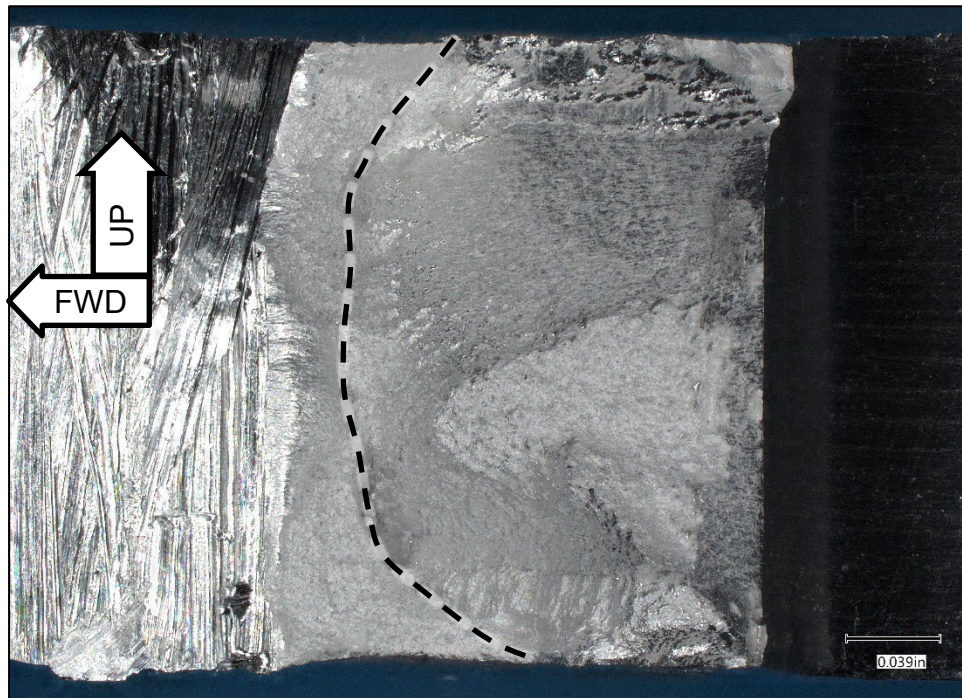


Figure C11. Optical image of the opened crack after oxide removal. A dashed line indicates the approximate crack boundary before lab fracture.

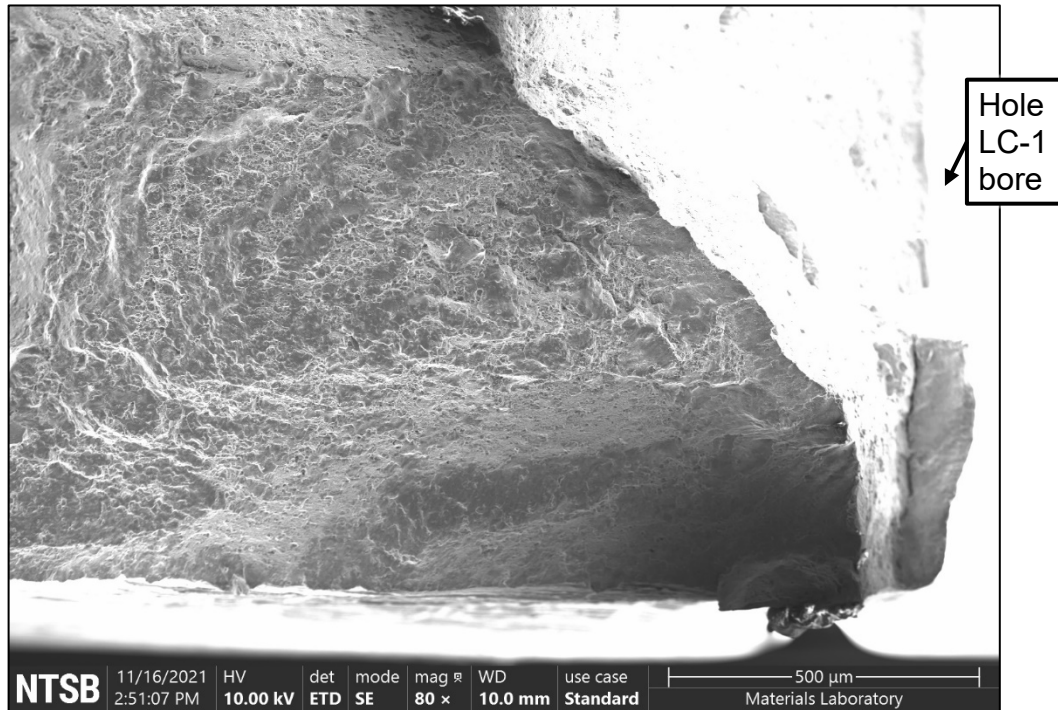


Figure C12. Fracture surface at the lower end of the crack after oxide removal.

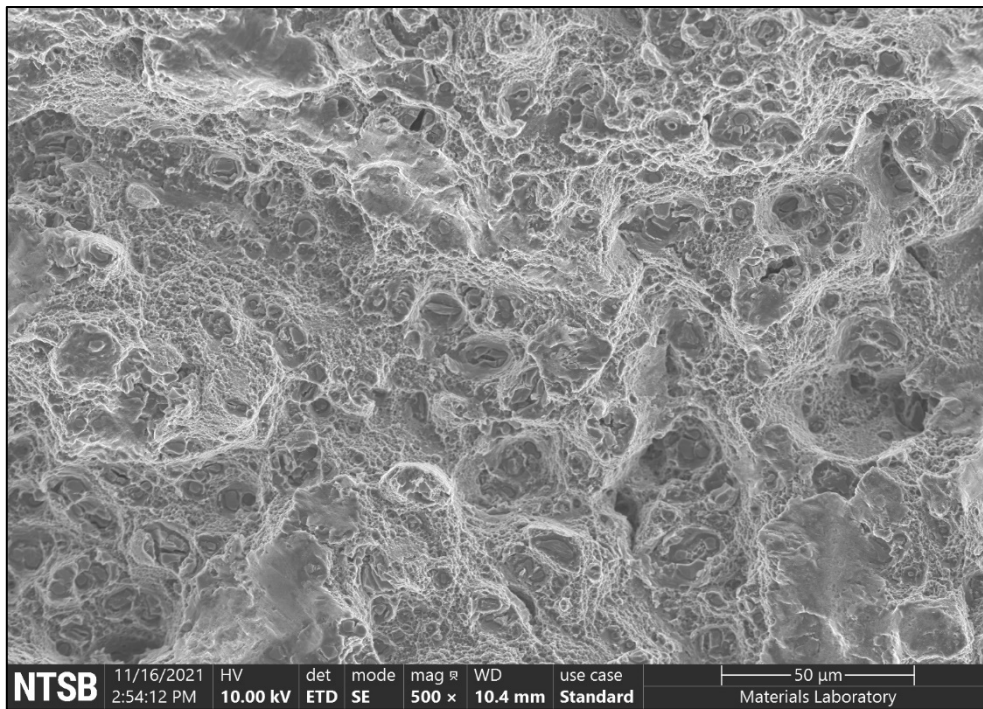


Figure C13. Ductile dimples observed on the crack fracture surface after oxide removal.

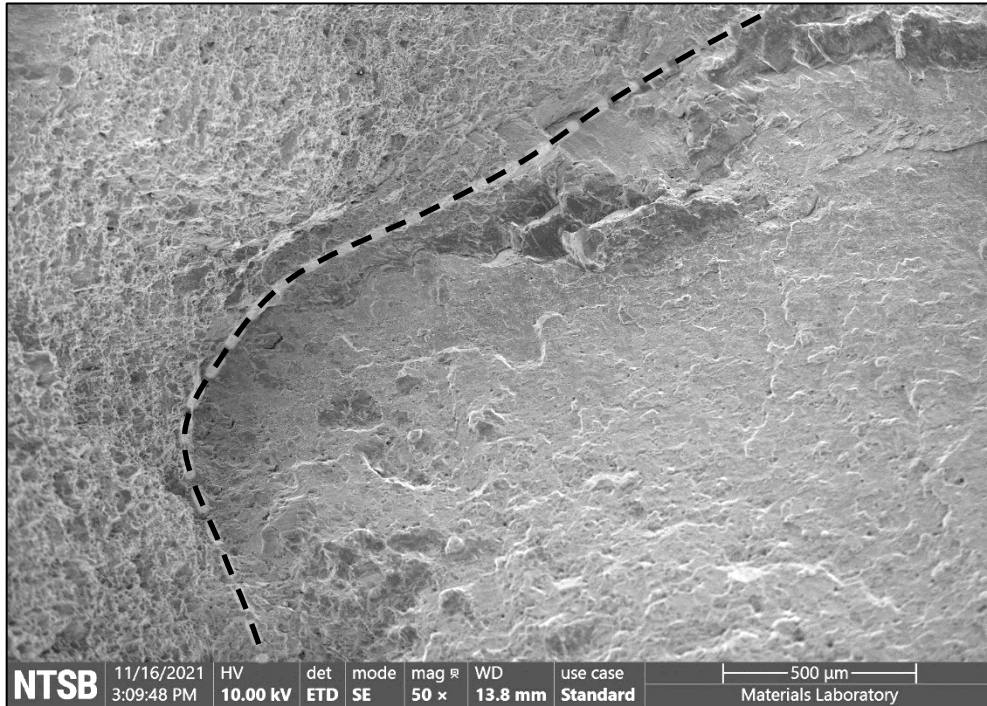


Figure C14. Fracture features at the crack boundary (dashed line) after oxide removal.

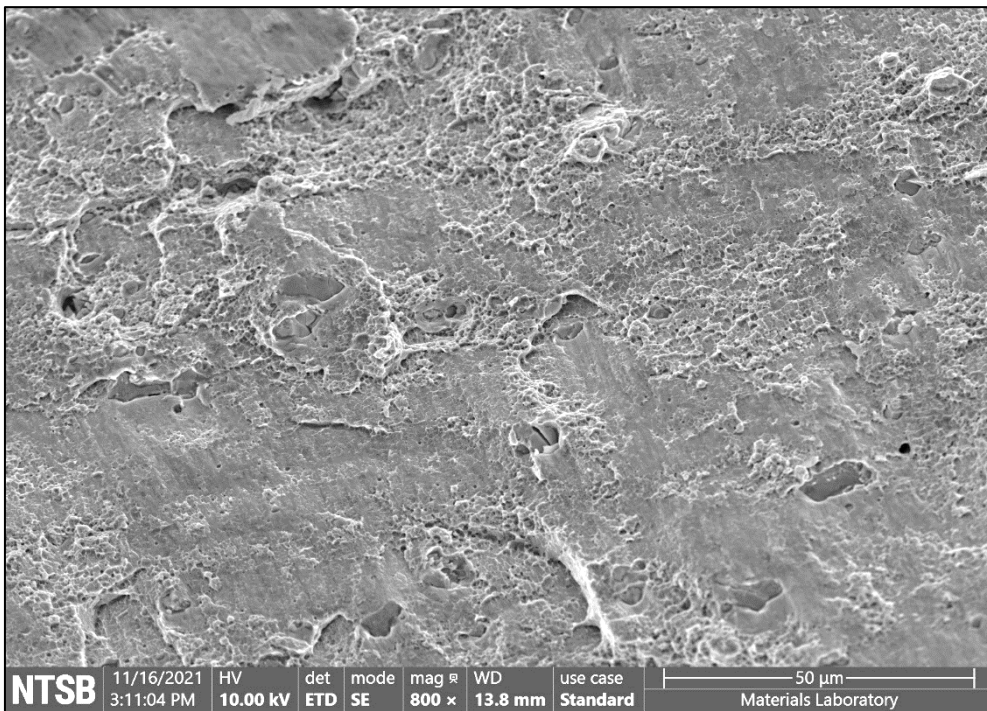


Figure C15. Dimples and sliding contact features near the crack boundary after oxide removal.